

000 001 002 003 004 005 006 007 008 009 010 011 012 013 014 015 016 017 018 019 020 021 022 023 024 025 026 027 028 029 030 031 032 033 034 035 036 037 038 039 040 041 042 043 044 045 046 047 048 049 050 051 052 053 ALIGNVID: TRAINING-FREE ATTENTION SCALING FOR SEMANTIC FIDELITY IN TEXT-GUIDED IMAGE- TO-VIDEO GENERATION

006 **Anonymous authors**

007 Paper under double-blind review

010 ABSTRACT

013 Text-guided image-to-video (TI2V) generation has recently achieved remarkable
014 progress, particularly in maintaining subject consistency and temporal coherence.
015 However, existing methods still struggle to adhere to fine-grained prompt seman-
016 tics, especially when prompts entail substantial transformations of the input image
017 (e.g., object addition, deletion, or modification), a shortcoming we term **semantic**
018 **negligence**. In a pilot study, we find that applying a Gaussian blur to the input im-
019 age improves semantic adherence. Analyzing attention maps, we observe clearer
020 foreground–background separation. From an energy perspective, this corresponds
021 to a lower-entropy cross-attention distribution. Motivated by this, we introduce
022 **AlignVid**, a training-free framework with two components: (i) *Attention Scaling*
023 *Modulation (ASM)*, which directly reweights attention via lightweight Q/K scal-
024 ing, and (ii) *Guidance Scheduling (GS)*, which applies ASM selectively across
025 transformer blocks and denoising steps to reduce visual quality degradation. This
026 minimal intervention improves prompt adherence while limiting aesthetic degra-
027 dation. In addition, we introduce **OmitI2V** to evaluate semantic negligence in
028 TI2V generation, comprising 367 human-annotated samples that span addition,
029 deletion, and modification scenarios. Extensive experiments demonstrate that
030 AlignVid can enhance semantic fidelity. Code and benchmark will be released.

031 1 INTRODUCTION

032 Image-to-video (I2V) generation aims to generate a temporally coherent video sequence from a static
033 image. Early I2V methods predominantly focused on short-term motion extrapolation (Blattmann
034 et al., 2023; Wang et al., 2023a; Xing et al., 2024; Chen et al., 2023; Zhang et al., 2023; Zeng et al.,
035 2024). More recently, text-guided image-to-video (TI2V) extends this setting by conditioning the
036 generative process on textual prompts alongside the source image, enabling fine-grained control over
037 motion semantics and temporal dynamics (Kong et al., 2024; Wan et al., 2025; Chen et al., 2025;
038 Zhang & Agrawala, 2025; Xu et al., 2024). However, current TI2V methods still fail to adhere to
039 fine-grained prompt semantics, particularly when prompts prescribe substantial transformations of
040 the source image (e.g., adding, deleting, or modifying objects). As illustrated in Figure 1, given the
041 prompt “*A sunflower grows in front of the house*”, the generated video preserves the image without
042 inserting the sunflower, indicating a misalignment between the prompt and the generated video.

043 To better understand this phenomenon, we conduct a pilot study and find that introducing Gaus-
044 sian noise to the input image unexpectedly improves both semantic fidelity and motion dynamics
045 (Figure 2). Analyzing the attention maps of TI2V models, we observe that Gaussian perturbations
046 increase foreground–background contrast, thereby amplifying the influence of textual prompts on
047 semantic changes. However, such naive perturbations inevitably degrade visual quality, raising a
048 key research question: *Can we directly regulate the model’s attention distribution—without altering*
049 *the user’s input—to enhance semantic alignment while preserving visual fidelity?*

050 To this end, we revisit the attention mechanism from an energy-based perspective. Prior work (Hong,
051 2024) shows that attention can be viewed as a gradient step that minimizes an underlying energy
052 function. Motivated by this formulation and by our observation that pretrained TI2V models al-
053 ready exhibit a coarse foreground–background separation in attention maps, we propose **AlignVid**,



Figure 1: The baseline model (FramePack) exhibits *semantic negligence*, failing to realize the prompt-specified modifications. In (a), the sunflower mentioned in the prompt is entirely missing. In (b), the person remains static instead of climbing onto the tank as instructed.

a training-free method for improving semantic alignment through minimal intervention. Specifically, AlignVid comprises two components: (i) *Attention Scaling Modulation (ASM)*, which rescales query or key representations, flattening the energy landscape and yielding a more concentrated, lower-entropy attention distribution; and (ii) *Guidance Scheduling (GS)*, which activates ASM selectively across transformer blocks and denoising steps to stabilize generation and mitigate visual-quality degradation. AlignVid enhances semantic adherence without retraining, relying only on lightweight modifications to the attention mechanism with negligible computational overhead.

To evaluate semantic negligence, we introduce **OmitI2V**, a benchmark focused on TI2V semantic adherence. It comprises 367 human-annotated samples across modification, addition, and deletion, and employs a VQA-based evaluation protocol for measuring semantic fidelity.

Our main contributions can be summarized as: (i) **Problem analysis.** We formalize *semantic negligence* in TI2V and, under an energy-based view, empirically link attention concentration (lower entropy) to semantic fidelity. (ii) **Method—AlignVid.** We propose a training-free framework that modulates attention via ASM with GS across blocks and steps, improving semantic fidelity with negligible computational overhead and minimal aesthetic impact. (iii) **Benchmark—OmitI2V.** We curate a dedicated benchmark with 367 human-annotated cases spanning modification, addition, and deletion, and adopt a VQA-based protocol to assess semantic fidelity.

2 RELATED WORKS

Image-to-Video Diffusion Models. I2V generation models can be broadly classified into GAN-based, Stable Diffusion-based, and DiT-based paradigms. GAN-based methods (Tulyakov et al., 2017; Skorokhodov et al., 2022; Tu et al., 2021) typically employ conditional GANs to generate videos from static images but often suffer from inherent challenges in modeling long-term dependencies and high-frequency details. Stable Diffusion-based models leverage UNet architectures. VideoComposer (Wang et al., 2023a) first integrates image conditioning into 3D-UNet by concatenating clean image latents with noisy video latents. Building on this, SVD (Blattmann et al., 2023) and DynamiCrafter (Xing et al., 2024) inject CLIP (Radford et al., 2021) features from reference images into the denoising process to enhance guidance. Further works explore cascading diffusion framework (Zhang et al., 2023) and leverage first and last frames to improve temporal coherence (Chen et al., 2023; Zeng et al., 2024). DiT-based methods (Brooks et al., 2024; Yang et al., 2024; Polyak et al., 2024; Ma et al., 2024; Kong et al., 2024; Wan et al., 2025) replace U-Net with Transformers by partitioning latent space frame patches into tokens for unified modeling of long-range dependencies. Recent advances (Chen et al., 2025; Zhang & Agrawala, 2025; Xu et al., 2024; Kong et al., 2024; Wan et al., 2025) employ multimodal fusion to align generated frames with visual and text inputs, significantly improving temporal consistency and narrative coherence.

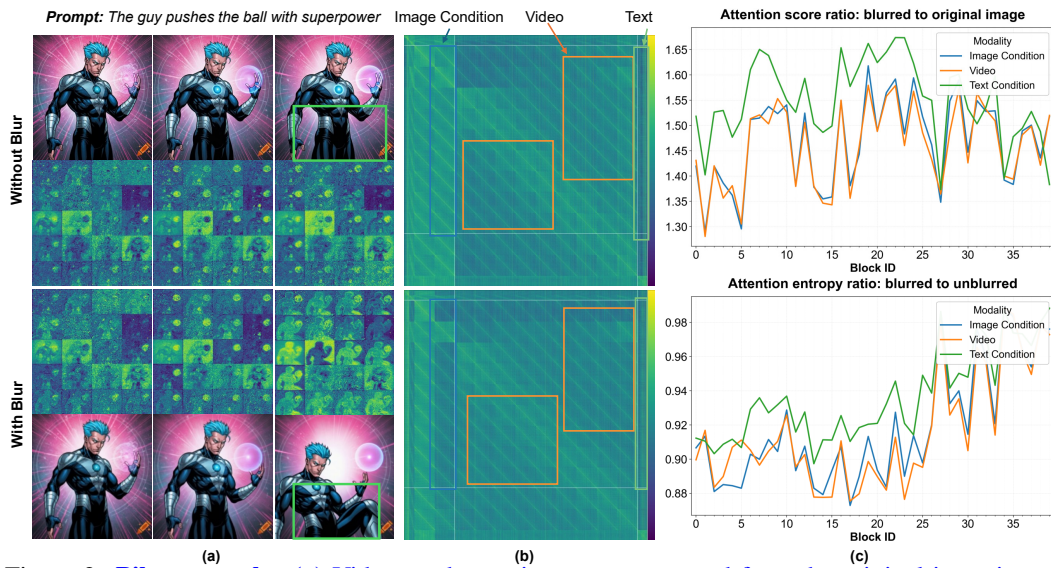


Figure 2: **Pilot example.** (a) Videos and attention maps generated from the original input image (top) and from the same image after applying Gaussian blur (bottom). (b) Attention map visualization. For the original input, the model assigns high attention scores to the reference image, low scores to the text tokens, and weak attention across video frames. When the blurred image is used as input, attention to the image is suppressed, while attention to the text and temporal neighbors is strengthened. (c) Statistics over 30 sampled benchmark examples, comparing attention scores in different regions before and after blur (top), as well as the ratio of attention entropy. Adding blur can increase cross-attention score while reducing entropy, indicating sharper and focused attention.

Image-to-Video Generation Benchmarks. Existing benchmarks for Image-to-Video (I2V) generation have primarily focused on evaluating the quality and consistency of the generated videos. VBench (Huang et al., 2024; Zheng et al., 2025) introduces comprehensive suites for assessing video generation models across various aspects, including temporal consistency, object permanence, and motion realism. In contrast, AIGCBench (Fan et al., 2023) and EvalCrafter (Liu et al., 2024c) focus on aspects such as text-video alignment and aesthetic quality. Other works have targeted more specific attributes of I2V generation. For instance, temporal compositionality (Feng et al., 2024), visual consistency (Wang et al., 2025) and precise motion control (Ren et al., 2024; Zhang et al., 2025). While existing benchmarks assess overall video quality and alignment, they do not capture *semantic negligence*, i.e., failures to follow explicit instructions for modification or addition. To address this gap, we introduce **OmitI2V**, the first benchmark tailored to semantic negligence in TI2V generation.

3 PILOT OBSERVATION ABOUT SEMANTIC NEGLIGENCE

We investigate the phenomenon of *semantic negligence* using the **OmitI2V** benchmark (details in Section 6). OmitI2V covers *modification*, *addition*, and *deletion* cases and uses a VQA-based protocol to assess semantic fidelity. We summarize two empirical observations:

Observation 1: Semantic negligence is prevalent in TI2V models. As summarized in Table 1, state-of-the-art methods often preserve the source image semantics instead of implementing the requested changes, indicating a misalignment between the textual instruction and the generated video.

Observation 2: Image perturbations can modulate attention and improve semantic fidelity. In a pilot study with FramePack F1 (Zhang & Agrawala, 2025), a slight Gaussian blur applied to the reference image reshapes the attention patterns. Qualitatively, Figure 2 shows that blur sharpens the separation between foreground and background and leads to more faithful action rendering. Quantitatively, we analyze attention on 30 sampled OmitI2V examples and compare attention statistics before and after blur. We measure (i) the average cross-attention strength from video queries to text tokens and to image tokens, and (ii) the entropy of the conditioning block (text + image tokens). Across samples, Gaussian blur consistently *increases* video→text cross-attention scores, *decreases* attention to background image regions, and *reduces* the conditioning-block entropy (i.e., $H_{\text{blur}}/H_{\text{clean}} < 1$), indicating sharper and more focused attention toward prompt-relevant tokens.

Motivated by these observations, we hypothesize that modulating attention can mitigate semantic negligence, while not precluding alternative explanations (e.g., capacity limits or training bias). However, steering attention by editing the inputs is impractical: image edits often degrade image quality. **This leads to our central question:** *Can we directly modulate the model’s attention, without modifying the original inputs, to improve semantic alignment while preserving visual fidelity?*

4 ATTENTION ENERGY IN DiT-BASED VIDEO DIFFUSION

4.1 PRELIMINARIES

We adopt an idealized view of a single attention head inside a DiT or MMDiT block and study how scaling the logits of different key groups (text, image, video) affects the attention distribution. At denoising step t , we write $Q_t \in \mathbb{R}^{n \times d}$, $K_t \in \mathbb{R}^{m \times d}$, $V_t \in \mathbb{R}^{m \times d_v}$ and define

$$Z_t = \frac{1}{\sqrt{d}} Q_t K_t^\top, \quad \text{Attn}(Q_t, K_t, V_t) = \sigma(Z_t) V_t, \quad (1)$$

where $\sigma(\cdot)$ denotes the row-wise softmax. Video queries can attend to keys from text, image, and video tokens. We denote a disjoint partition of key indices by

$$\mathcal{I}_{\text{text}}, \mathcal{I}_{\text{img}}, \mathcal{I}_{\text{vid}} \subseteq \{1, \dots, m\}, \quad (2)$$

and write $K_t = [K_t^{\text{text}}; K_t^{\text{img}}; K_t^{\text{vid}}]$ (up to permutation), which covers both standard DiT and MMDiT architectures. In Ti2V, the three groups play different roles: text tokens encode the desired edit, image tokens encode the input frame prior, and video tokens enforce temporal smoothness.

Energy view and entropy. For the i -th query, let $z^{(i)} \in \mathbb{R}^m$ be the corresponding logits. The log-partition and attention distribution are

$$\Phi(z^{(i)}) = \log \sum_j e^{z_j^{(i)}}, \quad p^{(i)} = \nabla_{z^{(i)}} \Phi = \sigma(z^{(i)}), \quad (3)$$

with Hessian $\nabla_{z^{(i)}}^2 \Phi = \text{Diag}(p^{(i)}) - p^{(i)} p^{(i)\top} \succeq 0$ which characterizes the sensitivity of attention probabilities to logit perturbations.

To quantify uncertainty within a subset of keys $S \subseteq \{1, \dots, m\}$, we define the restricted softmax and its entropy under inverse temperature $\alpha > 0$ as

$$p_{S,j}^{(i)}(\alpha) = \frac{e^{\alpha z_j^{(i)}}}{\sum_{k \in S} e^{\alpha z_k^{(i)}}}, \quad H_{i,S}(\alpha) = - \sum_{j \in S} p_{S,j}^{(i)}(\alpha) \log p_{S,j}^{(i)}(\alpha). \quad (4)$$

In a high-conflict prompt setting, we empirically observe that attention shifts towards the image prior and away from the text, while video-to-video attention also weakens. This explains semantic negligence: video queries mainly preserve the input instead of committing to the requested edit.

4.2 TEMPERATURE VIEW OF Q/K SCALING

Lemma 4.1 (Q/K scaling as temperature control). *Consider scaling the query or key embeddings by a positive scalar $\gamma_t > 0$. Replacing Q_t by $\gamma_t Q_t$ (or K_t by $\gamma_t K_t$) yields*

$$Z'_t = \frac{1}{\sqrt{d}} Q'_t K_t^\top = \gamma_t Z_t \quad (\text{or } Z'_t = \frac{1}{\sqrt{d}} Q_t K'_t^\top = \gamma_t Z_t), \quad (5)$$

so each row of the attention uses a softmax with temperature $\alpha_t = \gamma_t$, i.e. $p^{(i)}(\alpha_t) = \sigma(\alpha_t z^{(i)})$.

In multi-modal attention, we are interested in scaling only conditioning tokens. Let $S_{\text{cond}} = \mathcal{I}_{\text{text}} \cup \mathcal{I}_{\text{img}}$ denote the conditioning block, and keep video keys unscaled. Conceptually, increasing the temperature on S_{cond} both increases the total attention mass allocated to conditioning tokens relative to video self-attention and reshapes how attention is distributed within the conditioning block.

4.3 ENTROPY AND SEMANTIC FIDELITY

We now relate temperature scaling to entropy reduction and semantic fidelity.

216 **Lemma 4.2 (Within-block entropy monotonicity).** For any query i , subset S of key, and $\alpha > 0$,

$$218 \quad \frac{d}{d\alpha} H_{i,S}(\alpha) = -\alpha \text{Var}_{p_S^{(i)}(\alpha)}[z_S^{(i)}] \leq 0, \quad (6)$$

220 where the variance is taken with respect to $p_S^{(i)}(\alpha)$. Thus increasing α monotonically reduces the
221 entropy within S unless the logits $\{z_j^{(i)} : j \in S\}$ are degenerate.

223 Taking $S = S_{\text{cond}}$ shows that increasing α_t^{cond} yields a more concentrated attention distribution over
224 conditioning tokens for each video query, i.e., it reduces the uncertainty about which conditioning
225 tokens the query attends to, while leaving video self-attention unchanged.

226 **TI2V semantic fidelity.** From a mathematical view, entropy reduction is the direct consequence of
227 increasing the inverse temperature. From a signal-level viewpoint, the same temperature scaling acts
228 as a *semantic sharpening* operation on the softmax: as α increases, probability mass is reallocated
229 from low-logit tokens to a few high-logit tokens that carry stronger semantic evidence, while weak,
230 distracting tokens are suppressed. In our TI2V setting, semantic negligence manifests as a signal
231 imbalance, where attention overemphasizes the image prior and underweights edit-related text and
232 temporal cues, leading the model to preserve the input frame instead of realizing the requested edit.
233 Softmax sharpening, which theoretically corresponds to a reduction in attention entropy, serves as a
234 signal gain mechanism to resolve the condition conflict. By scaling the logits of the relevant token
235 blocks, we compel the video queries to shift their focus from the dominant image condition to the
236 magnified text signal, directly enhancing semantic compliance.

237 **Curvature and over-concentration.** For completeness, consider scaling all logits of a query by a
238 common factor $\alpha > 0$ and define $\Phi_i(\alpha) = \Phi(\alpha z^{(i)})$ with Hessian

$$239 \quad \mathcal{H}_i(\alpha) = \nabla_{z^{(i)}}^2 \Phi(\alpha z^{(i)}) = \alpha^2 \left(\text{Diag}(p^{(i)}(\alpha)) - p^{(i)}(\alpha) p^{(i)}(\alpha)^\top \right), \quad (7)$$

240 where $p^{(i)}(\alpha) = \sigma(\alpha z^{(i)})$. If Δ_i denotes the gap between the largest and second-largest logits in
241 $z^{(i)}$, one can show that for sufficiently large α the spectral norm $\|\mathcal{H}_i(\alpha)\|_{\text{spec}}$ eventually decreases
242 and converges to zero (proof in the supplementary material). Intuitively, very large temperatures
243 collapse attention onto a single token and flatten the energy landscape along off-peak directions.

244 **Design implications for TI2V.** Based on the above analysis, we summarize the design principles
245 that guide our method. (i) **Temperature as an attention gain knob.** Scaling Q or K is exactly
246 inverse-temperature control and thus offers an explicit way to strengthen or weaken the influence of
247 selected token groups without modifying the inputs. (ii) **Entropy reduction as decisive semantic
248 selection.** Increasing the temperature on a token block reduces its internal entropy and sharpens
249 attention onto a small set of high-logit, semantically relevant tokens.

251 5 METHOD

252 Building on the above analysis, we propose **AlignVid**, a training-free approach for modulating
253 attention distributions in DiT-based TI2V models. AlignVid has two components: (i) **Attention Scal-
254 ing Modulation (ASM)**, a lightweight mechanism that sharpens prompt-relevant attention; and (ii)
255 **Guidance Scheduling (GS)**, which selectively applies ASM across blocks and denoising steps to
256 preserve visual fidelity while improving semantic adherence. The method adds negligible overhead.
257 The pseudocode of AlignVid is provided in Algorithm 1 and Algorithm 2 (Appendix).

258 5.1 ATTENTION SCALING MODULATION

259 A straightforward way to sharpen attention is to inject external masks. However, this has three
260 drawbacks: (i) masks are static and misaligned with the evolving denoising dynamics; (ii) in open-
261 vocabulary settings, defining reliable masks (e.g., for unseen objects) is brittle; and (iii) maintaining
262 and applying masks adds inference overhead. To overcome these limitations, we introduce **Atten-
263 tion Scaling Modulation (ASM)**, which directly modifies the attention computation by scaling the
264 **query** or **key** embeddings within attention layers. Formally, let $Q \in \mathbb{R}^{n_q \times d_k}$, $K \in \mathbb{R}^{n_k \times d_k}$, and
265 $V \in \mathbb{R}^{n_k \times d_v}$. ASM modifies attention by scaling the query or key embeddings before the attention:

$$266 \quad \text{Attention}_{\text{ASM}}(Q, K, V) = \text{softmax} \left(\frac{Q' (K')^\top}{\sqrt{d_k}} \right) V, \quad (8)$$

270 where Q' and K' are the modulated embeddings. By *Lemma 4.1*, such scaling is equivalent to
 271 reparameterizing the row-wise softmax via its inverse temperature α .

272 **(S1) Scalar scaling.** Apply a multiplicative scalar $\gamma_s > 1$ to either Q or K :

$$274 \quad Q' = \gamma_s Q \quad \text{or} \quad K' = \gamma_s K. \quad (9)$$

275 This sharpens the attention by amplifying the contrast between relevant and irrelevant regions.

276 **(S2). Energy-based scaling.** Inspired by the energy interpretation of attention, we adaptively set
 277 the scaling coefficient according to the sharpness of the logits:

$$279 \quad \gamma_e = f\left(\frac{1}{n_q n_k} \sum_{i,j} \frac{Q_i K_j^\top}{\sqrt{d_k}}\right), \quad (10)$$

282 where $f(\cdot)$ is a monotonic function (e.g., sigmoid-normalized rescaling) and n_q, n_k denote
 283 query/key counts. This encourages stronger modulation when attention logits are diffuse.

284 285 5.2 GUIDANCE SCHEDULING

286 While ASM enhances semantic consistency, applying it indiscriminately across all blocks and steps
 287 may downgrade perceptual quality. We therefore introduce **Guidance Scheduling (GS)**, which
 288 gates ASM at the block level and along the denoising trajectory.

289 **Block-level Guidance Scheduling (BGS).** We observe that different transformer blocks contribute
 290 unequally: some focus more on foreground semantics, while others capture background context. We
 291 selectively apply attention modulation only to *foreground-sensitive* blocks. To identify *foreground-
 292 sensitive* blocks, we perform a lightweight calibration: collect attention maps on a small validation
 293 set, project them via PCA to capture dominant directions, and use an off-the-shelf grounding model
 294 to separate foreground from background. For each block l , we compute its *foreground ratio* $r^{(l)}$, the
 295 average fraction of attention mass allocated to foreground tokens. Blocks with $r^{(l)} > \tau$ (0.5) are
 296 deemed foreground-sensitive. We assign each block a scaling coefficient:

$$298 \quad g^{(l)} = \begin{cases} \gamma & \text{if } r^{(l)} > \tau \\ 1 & \text{otherwise,} \end{cases} \quad (11)$$

300 where $\gamma > 1$ controls the perturbation strength. The modulated attention is then apply:

$$302 \quad \text{Attention}^{(l)}(Q, K, V) = \text{softmax}\left(\frac{Q(g^{(l)} K)^\top}{\sqrt{d_k}}\right) V. \quad (12)$$

304 Empirically, we find that most foreground-sensitive blocks lie in the earlier half of the network.
 305 Consequently, we consider two variants of BGS in our experiments: (i) using the calibrated set of
 306 blocks with $r^{(l)} > \tau$, and (ii) a simpler heuristic that applies modulation to the first 50% of blocks.

307 **Step-level Guidance Scheduling (SGS).** We further specify *when* modulation is applied along the
 308 denoising process. Early steps operate under high noise and determine global semantic alignment,
 309 mid steps refine coarse structures, while late steps mainly enhance visual details. Formally, let
 310 $t \in \{1, 2, \dots, T\}$ denote the denoising step. We define a scheduling function:

$$312 \quad m(t) = \begin{cases} 1 & \text{if } t \in [t_{\text{low}}, t_{\text{high}}], \\ 0 & \text{otherwise,} \end{cases} \quad (13)$$

314 where $[t_{\text{low}}, t_{\text{high}}]$ denotes the interval of active guidance. To account for implementation differences
 315 (scaling either queries or keys), we combine block and step scheduling with an explicit scaling
 316 target. Let $s_Q, s_K \in \{0, 1\}$ indicate whether we scale queries or keys ($s_Q + s_K = 1$). We define:

$$317 \quad g^{(l,t)} = m(t) b^{(l)} (\gamma - 1), \quad (14)$$

319 where $b^{(l)}$ is the block gate and $m(t) \in \{0, 1\}$ the step mask. Then:

$$320 \quad Q'^{(l,t)} = (1 + s_Q \times g^{(l,t)}) Q^{(l)}, \quad K'^{(l,t)} = (1 + s_K \times g^{(l,t)}) K^{(l)}. \quad (15)$$

322 The scheduled attention is:

$$323 \quad \text{Attention}_t^{(l)} = \text{softmax}\left(\frac{Q'^{(l,t)} (K'^{(l,t)})^\top}{\sqrt{d_k}}\right) V^{(l)}. \quad (16)$$

324 325 326 327 328 329 330 331	Method	Semantic Alignment Evaluation			Visual Quality Evaluation	
		Modification \uparrow	Addition \uparrow	Deletion \uparrow	Dynamic Degree \uparrow	Aesthetic Quality \uparrow
Hunyuan I2V (Kong et al., 2024)		63.28	60.34	61.94	17.74	62.04
Wan 2.1 (Wan et al., 2025)		72.35	71.75	63.13	46.02	63.12
Skyreels-v2-I2V (Chen et al., 2025)		70.02	76.64	62.95	51.16	58.94
Skyreels-v2-DF (Chen et al., 2025)		71.10	73.28	65.35	47.30	61.10
FramePack (Zhang & Agrawala, 2025)		64.99	68.55	58.14	20.05	63.94
FramePack F1 (Zhang & Agrawala, 2025)		64.45	67.79	58.50	24.42	63.10
EasyAnimate (Xu et al., 2024)		65.53	67.18	60.89	45.76	61.41

Table 1: **Quantitative comparison on OmitI2V benchmark.** Comparison of state-of-the-art open-source TI2V models shows that semantic negligence remains prevalent.

334 335 336 337 338	Method	Semantic Alignment Evaluation			ViCLIP Score			Visual Quality Evaluation	
		Modification \uparrow	Addition \uparrow	Deletion \uparrow	Modification \uparrow	Addition \uparrow	Deletion \uparrow	Dynamic Degree \uparrow	Aesthetic Quality \uparrow
FramePack		64.99	68.55	58.14	20.83	21.08	20.43	20.05	63.94
FramePack + Ours		68.22 (+3.23)	73.13 (+4.58)	60.21 (+2.07)	21.25 (+0.42)	22.08 (+0.83)	20.86 (+0.43)	28.53 (+8.48)	63.57 (-0.37)
FramePack F1		64.45	67.79	58.50	21.06	19.91	20.61	24.42	63.10
FramePack F1 + Ours		71.27 (+6.82)	71.60 (+3.81)	61.06 (+2.56)	21.78 (+0.72)	21.04 (+1.13)	20.99 (+0.38)	33.16 (+8.74)	62.10 (-1.00)
Wan2.1		72.35	71.75	63.13	20.93	20.59	20.82	46.02	63.12
Wan2.1 + Ours		77.20 (+4.85)	79.54 (+7.79)	69.47 (+6.34)	22.19 (+1.26)	23.30 (+2.71)	21.29 (+0.47)	47.04 (+1.02)	61.63 (-1.49)

Table 2: **Effectiveness of our method.** Values in parentheses indicate relative improvement (%) over the corresponding baseline. Our method consistently boosts semantic alignment and motion dynamics with only marginal changes in aesthetic quality.

6 OMITI2V BENCHMARK

Existing image-to-video (I2V) benchmarks either lack explicit textual conditioning or assess only coarse text-image consistency, providing limited signal for fine-grained semantic fidelity. We introduce **OmitI2V**, a benchmark designed to evaluate whether TI2V models faithfully execute textual instructions that require *explicit visual edits* to the input image (modification, addition, deletion).

Evaluation axes. OmitI2V evaluates two complementary axes. (i) *Semantic Alignment Evaluation* evaluates whether the generated video realizes the prompt-specified edit under the three scenarios. We assess edit-level compliance with a VQA-based yes/no protocol and report accuracy. (ii) *Visual Quality Evaluation* reports the *dynamic degree* (the extent of motion) and *aesthetic quality* (perceptual fidelity and visual appeal), independent of semantic correctness.

Data and protocol. The benchmark contains **367** image–text pairs spanning diverse visual styles (real, synthetic, animation). Each pair is annotated with an edit type (*addition*, *deletion*, or *modification*) that specifies the intended visual change. Conventional metrics such as FVD are not designed to capture edit-level semantic compliance. Instead, for each generated video, we pose a structured yes/no question derived from the prompt and edit type (e.g., “*Did a sunflower appear in front of the house?*”) and compute accuracy using *Qwen2.5-VL-32B* (Wang et al., 2024). **We also employ the ViCLIP score (Wang et al., 2023b) as a text semantic matching metric for ablation experiments.**

7 EXPERIMENTS

7.1 EXPERIMENTAL SETUP

We evaluate semantic negligence in TI2V generation using our **OmitI2V** benchmark, which contains 367 annotated video-text pairs across modification, addition, and deletion scenarios. More experiments, including evaluations on other I2V benchmarks, hyperparameter ablations, efficiency comparisons, and qualitative visualizations, are provided in *appendix and supplementary material*.

Baseline models. We select two representative TI2V models to cover the main architectural lineages: **FramePack** (MM-DiT) (Zhang & Agrawala, 2025) concatenates multi-modal tokens, while **Wan2.1** (DiT) (Wan et al., 2025) factorizes image and text cross-attention.

Evaluation metrics. We adopt existing metrics from VBench (Huang et al., 2024), including dynamic degree and aesthetic quality, but exclude subject and background consistency due to the nature of addition/removal edits. To assess semantic alignment, we introduce a Visual Question Answering (VQA) protocol: a multimodal large language model (Qwen2.5-VL-32B) answers questions about the video content, providing an additional, interpretable measure of semantic correctness. We additionally employ the ViCLIP score as a text semantic matching metric for ablation experiments.

378 379 380 381 382 383 384	Method	Semantic Alignment Evaluation			ViCLIP Score			Visual Quality Evaluation	
		Modification \uparrow	Addition \uparrow	Deletion \uparrow	Modification \uparrow	Addition \uparrow	Deletion \uparrow	Dynamic Degree \uparrow	Aesthetic Quality \uparrow
<i>FramePack</i>									
Original	64.99	68.55	58.14	20.83	21.08	20.43	20.05	63.94	
Scalar scaling	67.15	73.44	59.86	21.38	22.03	21.05	28.28	63.41	
Energy-based modulation	66.61	72.37	58.66	<u>21.26</u>	21.79	<u>20.76</u>	26.48	63.62	
<i>Wan2.1</i>									
Original	72.35	71.75	63.13	20.93	20.59	20.82	46.02	63.12	
Scalar scaling	72.53	80.76	70.33	22.28	23.50	21.26	53.21	62.38	
Energy-based modulation	72.40	75.65	67.86	<u>21.56</u>	21.82	<u>20.97</u>	48.90	62.67	

385 Table 3: **Ablation about modulation variants.** Bold values denote the best performance.

386 387 388 389 390 391 392 393 394 395 396	Method	Semantic Alignment Evaluation			ViCLIP Score			Visual Quality Evaluation	
		Modification \uparrow	Addition \uparrow	Deletion \uparrow	Modification \uparrow	Addition \uparrow	Deletion \uparrow	Dynamic Degree \uparrow	Aesthetic Quality \uparrow
<i>FramePack</i>									
-	64.99	68.55	58.14	20.83	21.08	20.43	20.05	63.94	
Key-image	64.45	61.07	52.93	<u>14.55</u>	<u>11.95</u>	<u>15.19</u>	6.94	24.63	
Key-text	<u>65.71</u>	62.90	65.81	<u>15.88</u>	<u>12.81</u>	<u>16.10</u>	14.91	24.81	
Key-image and Key-text	68.22	73.13	<u>60.21</u>	<u>21.25</u>	<u>22.08</u>	20.86	28.53	63.57	
<i>Wan2.1</i>									
-	72.35	71.75	63.13	20.93	20.59	20.82	46.02	63.12	
Key in Self-attention	67.32	66.87	65.18	<u>19.20</u>	<u>16.91</u>	<u>19.03</u>	58.87	47.10	
Query-image	76.48	<u>80.46</u>	65.18	<u>22.10</u>	<u>23.39</u>	21.69	51.67	61.20	
Key-image	69.48	75.42	64.49	21.14	21.41	21.03	48.33	<u>62.55</u>	
Query-text	72.71	77.25	<u>68.27</u>	<u>22.13</u>	22.78	<u>21.45</u>	<u>59.90</u>	61.62	
Key-text	71.45	78.17	67.41	21.82	22.88	<u>21.43</u>	55.53	61.46	
Key-image and Query-text	76.66	79.85	67.75	21.04	21.80	21.00	60.67	61.58	
Key-image and Key-text	73.79	78.18	66.04	22.06	23.20	21.48	43.19	62.86	
Query-image and Key-text	72.53	80.76	<u>70.33</u>	<u>22.28</u>	<u>23.50</u>	21.26	53.21	62.38	

397 Table 4: **Ablation on scaling positions.** For *FramePack*, image and text tokens are concatenated and
398 processed via self-attention, making scaling Q or K effectively equivalent (we scale K in practice).
399 For *Wan2.1*, video tokens use self-attention (treated as in *FramePack*), while image and text act
400 as cross-attention conditions where Q and K differ and must be analyzed separately. Bold and
401 underlined numbers denote the best and second-best scores, respectively.

402 7.2 COMPARISON EXPERIMENTS

404 **Semantic negligence remains prevalent.** Table 1 summarizes results on OmitI2V-Bench. There is
405 no existing TI2V model that could uniformly handles all edit types. For example, *Wan2.1* attains the
406 highest VQA-based accuracy on *modification* and *addition* but drops notably on *deletion*; *Skyreels-v2-I2V*
407 excels at *addition* yet is inconsistent elsewhere. *FramePack* (and its F1 variant), despite
408 strong autoregressive priors, shows the weakest semantic fidelity, particularly on *deletion*. These
409 patterns underscore that semantic negligence persists across architectures and edit categories.410 **Semantics-aesthetic trade-off.** Table 1 shows that stronger prompt adherence is not necessarily
411 aligned with higher visual quality. For instance, *EasyAnimate* and *Skyreels-v2-DF* attain competitive
412 dynamic degree and aesthetic scores, yet exhibit semantic omissions. This motivates the development
413 of methods that improve semantic alignment while minimizing visual-quality degradation.414 **Effectiveness of AlignVid.** Table 2 shows that plugging **AlignVid** into *FramePack*, *FramePack-F1*,
415 and *Wan2.1* yields consistent gains in semantic fidelity and dynamic degree across all edit types,
416 indicating good architectural generality. While aesthetic quality scores may drop slightly, the de-
417 crease is minor relative to the substantial improvements in semantic fidelity and motion coherence,
418 validating the design of selective attention scaling and scheduling.

420 7.3 ABLATION AND GENERALIZATION EXPERIMENT

422 **Ablation on modulation strategy.** Table 3 compares the proposed variants in Section 5.1: *scalar*
423 *scaling* and *energy-based modulation*. Both improve semantic fidelity across *modification*, *addition*,
424 and *deletion*, confirming that attention reweighting is effective. The energy-based variant yields
425 smaller drops in aesthetic quality but also smaller semantic gains. Considering its additional infer-
426 ence overhead, we adopt *scalar scaling* for the remainder of the experiments.427 **Ablation on scaling position.** We ablate scaling sites inside attention (queries (Q) and keys (K))
428 and their image/text partitions (Table 4). On *FramePack*, where image and text tokens are concate-
429 nated and processed via self-attention, scaling Q or K is effectively equivalent; empirically, com-
430 bining image- and text-side key scaling delivers the strongest overall semantic gains. In contrast,
431 key-image only provides limited benefits and can hurt aesthetic metrics. On *Wan2.1*, where video
tokens use self-attention but image/text act as cross-attention conditions, positions are no longer

432	BGS	SGS	Semantic Alignment Evaluation			ViCLIP Score			Visual Quality Evaluation	
			Modification \uparrow	Addition \uparrow	Deletion \uparrow	Modification \uparrow	Addition \uparrow	Deletion \uparrow	Dynamic Degree \uparrow	Aesthetic Quality \uparrow
FramePack										
434	-	-	64.99	68.55	58.14	20.83	21.08	20.43	20.05	63.94
435	All	Early Steps	67.15	73.44	59.86	21.38	22.03	21.05	28.28	63.41
436	All	Middle Steps	62.71	70.01	56.60	20.85	21.06	20.54	20.05	63.96
437	All	End Steps	64.63	69.62	57.63	20.80	21.08	20.47	19.54	63.94
438	All	All	69.84	76.03	59.86	21.56	22.30	21.31	32.13	61.56
439	Foreground-focus	Early Steps	68.22	73.13	60.21	21.25	22.08	20.86	28.53	63.57
440	Background-focus	Early Steps	66.25	69.16	56.26	20.88	21.03	20.50	17.99	64.02
441	First half blocks	Early Steps	66.61	73.89	58.31	20.68	22.16	20.76	25.96	63.58
442	Last half blocks	Early Steps	65.35	69.92	57.18	20.39	21.19	20.56	22.11	63.49
Wan2.1										
443	-	-	72.35	71.75	63.13	20.3	21.08	20.43	46.02	63.12
444	All	Early Steps	72.53	80.76	70.33	22.28	23.50	21.26	53.21	61.38
445	All	Middle Steps	68.76	74.81	61.41	21.37	21.22	20.89	42.16	62.91
446	All	End Steps	69.84	74.05	66.90	21.20	21.86	21.44	53.98	61.55
447	All	All	78.28	80.46	69.13	22.63	24.26	21.93	49.36	60.59
448	Foreground-focus	Early Steps	77.20	79.54	69.47	22.19	23.30	21.29	47.04	61.63
449	Background-focus	Early Steps	71.99	75.88	65.35	21.26	21.93	20.86	41.90	62.62
450	First half blocks	Early Steps	76.55	78.85	68.10	22.18	22.60	21.40	52.70	61.54
451	Last half blocks	Early Steps	73.68	77.89	62.64	20.63	22.48	21.20	50.31	61.47

Table 5: **Ablation of block- and step-level guidance scheduling.** Gating ASM to BGS boosts VQA-based semantic fidelity with minimal aesthetic impact. For SGS, early-step activation delivers the strongest semantic gains, mid/late activation better preserves aesthetics, and all-step activation maximizes fidelity but reduces visual quality. We therefore adopt an early-step schedule.

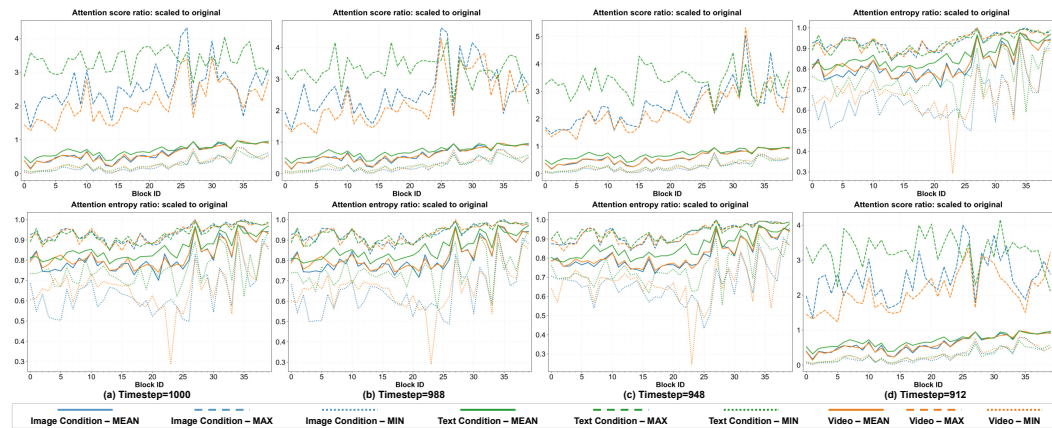


Figure 3: **Attention analysis.** ASM sharpens attention (lower entropy), boosts focus on text tokens and adjacent frames, and suppresses static-image regions.

symmetric: pairing image queries with text keys attains the best *addition/deletion* accuracy, pairing image keys with text queries yields the highest dynamic degree, and image keys with text keys offers the best aesthetic score. Overall, jointly modulating image- and text-side sites yields the best semantic–visual trade-off, with architecture-aware preferences between self- and cross-attention.

Ablation on block- and step-level guidance scheduling. We evaluate the proposed BGS and SGS strategy on *FramePack* and *Wan2.1*, as shown in Table 5. For BGS, limiting ASM to foreground-focused blocks improves semantic fidelity while mitigating aesthetic degradation by concentrating modulation where text–visual grounding is strongest. For SGS, activating guidance in early denoising steps yields the largest semantic gains; mid/late activation offers weaker semantic improvements but better preserves aesthetics. Enabling guidance at all steps maximizes semantic fidelity but incurs a noticeable visual quality drop (e.g., a 2.38% relative decrease for *FramePack*). Balancing these trade-offs, we adopt an early-step schedule by default.

Attention analysis. To better understand the effect of ASM, we further analyze attention maps before and after applying AlignVid on the benchmark, as illustrated in Figure 3. Concretely, we compute (i) attention distributions over different token groups, (ii) the ratio between the maximum attention scores, and (iii) the ratio of attention entropies for video queries. After modulation, the attention distributions become noticeably sharper, reflected by a consistent decrease in attention entropy. At the signal level, video queries allocate stronger attention to text tokens and temporally adjacent frames, and relatively less to static image regions, encouraging the model to focus more on prompt and temporal cues. This shift in attention patterns correlates well with the improved semantic consistency observed in the generated videos.

486	487	Method	Semantic Alignment Evaluation			ViCLIP Score			Visual Quality Evaluation	
			Modification \uparrow	Addition \uparrow	Deletion \uparrow	Modification \uparrow	Addition \uparrow	Deletion \uparrow	Dynamic Degree \uparrow	Aesthetic Quality \uparrow
488	489	CFG=1 (no cfg)	63.55	63.66	61.06	19.20	17.09	19.67	41.65	61.19
490	491	CFG=1 + AlignVid	65.88	72.52	60.21	19.51	18.47	19.89	42.48	62.11
492	493	CFG=5 (Official)	72.35	71.75	63.13	20.83	21.08	20.43	46.02	63.12
493	494	CFG=5 + AlignVid	77.20	79.54	69.47	22.19	23.30	21.29	47.04	61.63

Table 6: Comparison with CFG on Wan2.1. AlignVid and CFG are complementary: applying AlignVid on top of CFG consistently boosts semantic alignment across all edit types for both weak guidance (CFG=1) and strong guidance (CFG=5), while maintaining comparable visual quality.

494	495	496	497	Method	Single object	Two object	Counting	Colors	Position	Color attribution	Aesthetic Score
498	499	500	501	OmniGen2 (Wu et al., 2025)	0.99	0.94	0.67	0.85	0.55	0.62	5.517
499	500	501	502	+ AlignVid	1.00($+0.01$)	0.97($+0.03$)	0.52(-0.15)	0.89($+0.04$)	0.60($+0.05$)	0.70($+0.08$)	5.568($+0.05$)

Table 7: Quantitative results on GenEval. Prompt rewriter is not utilized during inference.

498	499	500	501	Model	Subject Consistency	Temporal Style	Temporal Flickering	Spatial Relationship	Scene	Overall Consistency	Object Class	Multiple Objects
498	499	500	501	Wan2.1-T2V-1.3B	94.24	22.67	99.32	72.74	19.62	23.59	79.03	53.35
499	500	501	502	+ AlignVid	94.51($+0.27$)	23.46($+0.79$)	98.66(-0.66)	84.25($+11.51$)	25.80($+6.18$)	24.47($+0.88$)	79.91($+0.88$)	66.46($+13.11$)
500	501	502	503	Model	Motion Smoothness	Imaging Quality	Dynamic Degree	Color	Background Consistency	Appearance Style	Aesthetic Quality	
500	501	502	503	Wan2.1-T2V-1.3B	97.77	69.70	70.83	88.08	98.09	19.58	64.60	
501	502	503	504	+ AlignVid	98.05($+0.28$)	68.53(-1.17)	68.06(-2.77)	91.80($+3.72$)	98.20($+0.11$)	20.16($+0.58$)	62.69(-1.91)	

Table 8: Quantitative results on VBenCh. AlignVid also yields gains in the T2V task.

503	504	505	506	Model	Add	Adjust	Extract	Replace	Remove	Background	Style	Compose	Action	Aesthetic Score
503	504	505	506	OmniGen2 (Wu et al., 2025)	2.52	3.27	2.08	3.12	2.83	3.65	4.57	2.89	4.59	5.606
504	505	506	507	+ AlignVid	3.53($+1.01$)	3.12(-0.15)	2.04(-0.04)	3.18($+0.06$)	3.33($+0.50$)	3.65	4.75($+0.18$)	2.43(-0.46)	4.50(-0.09)	5.624($+0.02$)

Table 9: Quantitative results on ImgEdit. AlignVid also yields gains in the image editing task.

Comparison with Classifier-Free Guidance (CFG). We also compare the proposed AlignVid with classifier-free guidance (CFG) in Wan2.1. As shown in Table 6, AlignVid and CFG are complementary: applying AlignVid on top of CFG further improves performance. Compared with CFG, AlignVid enjoys two practical advantages: (i) it requires no additional training, and (ii) it introduces negligible extra inference overhead (see the supplementary material for details).

Generalization: AlignVid on text-to-image generation. We further evaluate the generalization of AlignVid on text-to-image (T2I) generation, using OmniGen2 (Wu et al., 2025) as the baseline. As reported on the GenEval (Ghosh et al., 2024) in Table 7, incorporating AlignVid improves all metrics except *Counting*, indicating that our attention modulation can also transfer to the image domain.

Generalization: AlignVid on text-to-video (T2V) generation. We also evaluate AlignVid on T2V generation, using Wan2.1-T2V-1.3B (Wu et al., 2025) with a scale coefficient of 1.35. As reported on the VBenCh (Huang et al., 2024) benchmark in Table 8, integrating AlignVid improves most dimensions, while leading to decreases in *Temporal Flickering*, *Imaging Quality*, *Dynamic Degree*, and *Aesthetic Quality*. Some metrics appear to be closely coupled: when AlignVid encourages stronger motion and temporal changes, the resulting videos may exhibit mild motion blur, which can hurt perceived sharpness and aesthetic scores, even though the prompt adherence is improved.

Generalization: AlignVid on image editing. We also apply it to an image editing benchmark (ImgEdit (Ye et al., 2025)), using OmniGen2 (Wu et al., 2025) as the baseline model. As shown in Table 9, integrating AlignVid leads to consistent gains on several editing categories, including *Add*, *Replace*, *Remove*, and *Style*, and also improves the overall aesthetic score. Interestingly, this contrasts with our observations in video generation, where AlignVid slightly reduces aesthetic quality. A plausible explanation is that, in the video setting, stronger motion modeling tends to introduce additional motion blur, whereas static image editing is not subject to such temporal artifacts.

8 CONCLUSION

In this paper, to mitigate the challenge of *semantic negligence* in TI2V generation, we proposed **AlignVid**, a training-free method based on an energy-based perspective of attention. Our analysis links query/key scaling to a flatter energy landscape and a more concentrated attention distribution. The proposed method comprises *ASM* for attention rescaling and *GS* for selective deployment across transformer blocks and denoising steps. To facilitate evaluation, we provide **OmitI2V**, a benchmark consisting of 367 human-annotated samples across three scenarios, namely modification, addition, and deletion. Experiment results show that AlignVid yields consistent improvements in semantic fidelity and dynamic degree with limited aesthetic degradation.

540 **Ethics Statement.** We follow the ICLR Code of Ethics. Our study focuses on inference-time
 541 mechanisms for TI2V generation and does not involve personal data, sensitive attributes, or human
 542 subjects beyond internal annotation. The OmitI2V benchmark contains 367 image–text pairs curated
 543 from license-compliant sources and synthetic content. We exclude content that is violent, sexual,
 544 or otherwise harmful. Annotators were briefed with written guidelines, provided example cases,
 545 and compensated at or above local standards; no medical or biometric data were collected. While
 546 improving semantic adherence may increase the risk of misuse (e.g., misleading edits), our release
 547 includes a research-only license and usage terms prohibiting identity manipulation, harassment, or
 548 deception. The work complies with applicable policies on privacy, copyright, and research integrity.

549 **Reproducibility Statement.** The paper specifies *ASM* and *GS* with complete formulas and pseudo-
 550 code (Appendix F); the appendix details implementation notes (e.g., Q/K scaling, block/step
 551 gating). We will release code and data to reproduce all results. The appendix further includes
 552 evaluations on additional I2V benchmarks, hyperparameter ablations, efficiency comparisons, and
 553 qualitative visualizations. Representative video results are included in the supplementary materials.

555 REFERENCES

- 557 Hervé Abdi and Lynne J Williams. Principal component analysis. *Wiley interdisciplinary reviews: 558 computational statistics*, 2(4):433–459, 2010.
 559
- 560 Andreas Blattmann, Tim Dockhorn, Sumith Kulal, Daniel Mendelevitch, Maciej Kilian, Dominik
 561 Lorenz, Yam Levi, Zion English, Vikram Voleti, Adam Letts, Varun Jampani, and Robin Rom-
 562 bach. Stable Video Diffusion: Scaling Latent Video Diffusion Models to Large Datasets. *arXiv 563 preprint arXiv:2311.15127*, 2023.
- 564 Tim Brooks, Bill Peebles, Connor Holmes, Will DePue, Yufei Guo, Li Jing, David Schnurr, Joe
 565 Taylor, Troy Luhman, Eric Luhman, Clarence Ng, Ricky Wang, and Aditya Ramesh. Video
 566 Generation Models as World Simulators. 2024.
- 567 Minghong Cai, Xiaodong Cun, Xiaoyu Li, Wenze Liu, Zhaoyang Zhang, Yong Zhang, Ying Shan,
 568 and Xiangyu Yue. Dictrl: Exploring attention control in multi-modal diffusion transformer for
 569 tuning-free multi-prompt longer video generation. In *Proceedings of the Computer Vision and*
 570 *Pattern Recognition Conference*, pp. 7763–7772, 2025.
- 572 Mingdeng Cao, Xintao Wang, Zhongang Qi, Ying Shan, Xiaohu Qie, and Yinjiang Zheng. Mas-
 573 acrnl: Tuning-free mutual self-attention control for consistent image synthesis and editing. In
 574 *Proceedings of the IEEE/CVF international conference on computer vision*, pp. 22560–22570,
 575 2023.
- 576 Guibin Chen, Dixuan Lin, Jiangping Yang, Chunze Lin, Junchen Zhu, Mingyuan Fan, Hao Zhang,
 577 Sheng Chen, Zheng Chen, Chengcheng Ma, et al. Skyreels-v2: Infinite-length film generative
 578 model. *arXiv preprint arXiv:2504.13074*, 2025.
- 580 Xi Chen, Yutong Feng, Mengting Chen, et al. Zero-shot image editing with reference imitation.
 581 *arXiv preprint arXiv:2406.07547*, 2024.
- 583 Xinyuan Chen, Yaohui Wang, Lingjun Zhang, Shaobin Zhuang, Xin Ma, Jiashuo Yu, Yali Wang,
 584 Dahua Lin, Yu Qiao, and Ziwei Liu. SEINE: Short-to-Long Video Diffusion Model for Generative
 585 Transition and Prediction. In *ICCV*, 2023.
- 586 Fanda Fan, Chunjie Luo, Wanling Gao, and Jianfeng Zhan. Aigebench: Comprehensive eval-
 587 uation of image-to-video content generated by ai. *BenchCouncil Transactions on Benchmarks,
 588 Standards and Evaluations*, 3(4):100152, 2023. ISSN 2772-4859. doi: <https://doi.org/10.1016/j.tbench.2024.100152>. URL <https://www.sciencedirect.com/science/article/pii/S2772485924000048>.
- 592 Weixi Feng, Jiachen Li, Michael Saxon, Tsu-jui Fu, Wenhui Chen, and William Yang Wang. Tc-
 593 bench: Benchmarking temporal compositionality in text-to-video and image-to-video generation.
arXiv preprint arXiv:2406.08656, 2024.

- 594 Dhruba Ghosh, Hannaneh Hajishirzi, and Ludwig Schmidt. Geneval: An object-focused framework
 595 for evaluating text-to-image alignment. *Advances in Neural Information Processing Systems*, 36,
 596 2024.
- 597 Amir Hertz, Ron Mokady, Jay Tenenbaum, Kfir Aberman, Yael Pritch, and Daniel Cohen-Or.
 598 Prompt-to-prompt image editing with cross attention control. *arXiv preprint arXiv:2208.01626*,
 599 2022.
- 600 Susung Hong. Smoothed energy guidance: Guiding diffusion models with reduced energy curvature
 601 of attention. *Advances in Neural Information Processing Systems*, 37:66743–66772, 2024.
- 602 Ziqi Huang, Yinan He, Jiashuo Yu, Fan Zhang, Chenyang Si, Yuming Jiang, Yuanhan Zhang, Tianx-
 603 ing Wu, Qingyang Jin, Nattapol Chanpaisit, Yaohui Wang, Xinyuan Chen, Limin Wang, Dahua
 604 Lin, Yu Qiao, and Ziwei Liu. Vbench: Comprehensive benchmark suite for video generative mod-
 605 els. In *Proceedings of the IEEE/CVF Conference on Computer Vision and Pattern Recognition*
 606 (CVPR), pp. 21807–21818, June 2024.
- 607 Aaron Hurst, Adam Lerer, Adam P Goucher, Adam Perelman, Aditya Ramesh, Aidan Clark, AJ Os-
 608 trow, Akila Welihinda, Alan Hayes, Alec Radford, et al. Gpt-4o system card. *arXiv preprint*
 609 *arXiv:2410.21276*, 2024.
- 610 Shutong Jin, Ruiyu Wang, and Florian T. Pokorny. Realcraft: Attention control as a tool for zero-
 611 shot consistent video editing. In *arXiv preprint arXiv:2312.12635*, 2025.
- 612 Weijie Kong, Qi Tian, Zijian Zhang, Rox Min, Zuozhuo Dai, Jin Zhou, Jiangfeng Xiong, Xin Li,
 613 Bo Wu, Jianwei Zhang, et al. Hunyanvideo: A systematic framework for large video generative
 614 models. *arXiv preprint arXiv:2412.03603*, 2024.
- 615 Bingyan Liu, Chengyu Wang, Tingfeng Cao, Kui Jia, and Jun Huang. Towards understanding
 616 cross and self-attention in stable diffusion for text-guided image editing. In *arXiv preprint*
 617 *arXiv:2403.03431*, 2024a.
- 618 Shengyu Liu, Yifan Zhu, Yang Zhou, et al. Video-p2p: Video editing with cross-attention control. In
 619 *Proceedings of the IEEE/CVF Conference on Computer Vision and Pattern Recognition (CVPR)*,
 620 pp. 12164–12173, 2024b.
- 621 Yaofang Liu, Xiaodong Cun, Xuebo Liu, Xintao Wang, Yong Zhang, Haoxin Chen, Yang Liu,
 622 Tieyong Zeng, Raymond Chan, and Ying Shan. Evalcrafter: Benchmarking and evaluating large
 623 video generation models. In *Proceedings of the IEEE/CVF Conference on Computer Vision and*
 624 *Pattern Recognition (CVPR)*, pp. 22139–22149, June 2024c.
- 625 Xin Ma, Yaohui Wang, Gengyun Jia, Xinyuan Chen, Ziwei Liu, Yuan-Fang Li, Cunjian Chen,
 626 and Yu Qiao. Latte: Latent Diffusion Transformer for Video Generation. *arXiv preprint*
 627 *arXiv:2401.03048*, 2024.
- 628 Yue Ma, Xiaodong Cun, Sen Liang, et al. Magicstick: Controllable video editing via control handle
 629 transformations. In *arXiv preprint arXiv:2312.03047*, 2025.
- 630 Adam Polyak, Amit Zohar, Andrew Brown, Andros Tjandra, Animesh Sinha, Ann Lee, Apoorv
 631 Vyas, Bowen Shi, Chih-Yao Ma, Ching-Yao Chuang, et al. Movie gen: A cast of media foun-
 632 dation models. *arXiv preprint arXiv:2410.13720*, 2024.
- 633 Chenyang Qi, Xiaodong Cun, Yong Zhang, Chenyang Lei, Xintao Wang, Ying Shan, and Qifeng
 634 Chen. Fatezero: Fusing attentions for zero-shot text-based video editing. *arXiv:2303.09535*,
 635 2023.
- 636 Alec Radford, Jong Wook Kim, Chris Hallacy, Aditya Ramesh, Gabriel Goh, Sandhini Agar-
 637 wal, Girish Sastry, Amanda Askell, Pamela Mishkin, Jack Clark, Gretchen Krueger, and Ilya
 638 Sutskever. Learning Transferable Visual Models From Natural Language Supervision. In *ICML*,
 639 2021.
- 640 Nikhila Ravi, Valentin Gabeur, Yuan-Ting Hu, Ronghang Hu, Chaitanya Ryali, Tengyu Ma, Haitham
 641 Khedr, Roman Rädle, Chloe Rolland, Laura Gustafson, et al. Sam 2: Segment anything in images
 642 and videos. *arXiv preprint arXiv:2408.00714*, 2024.

- 648 Weiming Ren, Huan Yang, Ge Zhang, Cong Wei, Xinrun Du, Wenhao Huang, and Wenhua
 649 Chen. Consisti2v: Enhancing visual consistency for image-to-video generation. *arXiv preprint*
 650 *arXiv:2402.04324*, 2024.
- 651
- 652 Ivan Skorokhodov, Sergey Tulyakov, and Mohamed Elhoseiny. Stylegan-v: A continuous video
 653 generator with the price, image quality and perks of stylegan2. In *2022 IEEE/CVF Conference on*
 654 *Computer Vision and Pattern Recognition (CVPR)*, pp. 3616–3626, 2022.
- 655
- 656 Xiaoguang Tu, Yingtian Zou, Jian Zhao, Wenjie Ai, Jian Dong, Yuan Yao, Zhikang Wang, Guodong
 657 Guo, Zhifeng Li, Wei Liu, and Jia Shi Feng. Image-to-video generation via 3d facial dynamics,
 658 2021. URL <https://arxiv.org/abs/2105.14678>.
- 659
- 660 Sergey Tulyakov, Ming-Yu Liu, Xiaodong Yang, and Jan Kautz. Mocogan: Decomposing motion
 661 and content for video generation, 2017. URL <https://arxiv.org/abs/1707.04993>.
- 662
- 663 Team Wan, Ang Wang, Baole Ai, Bin Wen, Chaojie Mao, Chen-Wei Xie, Di Chen, Feiwu Yu,
 664 Haiming Zhao, Jianxiao Yang, et al. Wan: Open and advanced large-scale video generative
 665 models. *arXiv preprint arXiv:2503.20314*, 2025.
- 666
- 667 Jiarui Wang, Huiyu Duan, Ziheng Jia, Yu Zhao, Woo Yi Yang, Zicheng Zhang, Zijian Chen, Jun-
 668 tong Wang, Yuke Xing, Guangtao Zhai, et al. Love: Benchmarking and evaluating text-to-video
 669 generation and video-to-text interpretation. *arXiv preprint arXiv:2505.12098*, 2025.
- 670
- 671 Peng Wang, Shuai Bai, Sinan Tan, Shijie Wang, Zhihao Fan, Jinze Bai, Keqin Chen, Xuejing Liu,
 672 Jialin Wang, Wenbin Ge, et al. Qwen2-vl: Enhancing vision-language model’s perception of the
 673 world at any resolution. *arXiv preprint arXiv:2409.12191*, 2024.
- 674
- 675 Xiang Wang, Hangjie Yuan, Shiwei Zhang, Dayou Chen, Jiuniu Wang, Yingya Zhang, Yujun Shen,
 676 Deli Zhao, and Jingren Zhou. VideoComposer: Compositional Video Synthesis with Motion
 677 Controllability. In *NeurIPS*, 2023a.
- 678
- 679 Yi Wang, Yinan He, Yizhuo Li, Kunchang Li, Jiashuo Yu, Xin Ma, Xinhao Li, Guo Chen, Xinyuan
 680 Chen, Yaohui Wang, et al. Internvid: A large-scale video-text dataset for multimodal understand-
 681 ing and generation. *arXiv preprint arXiv:2307.06942*, 2023b.
- 682
- 683 Chenyuan Wu, Pengfei Zheng, Ruiran Yan, Shitao Xiao, Xin Luo, Yueze Wang, Wanli Li, Xiyan
 684 Jiang, Yexin Liu, Junjie Zhou, et al. Omnipgen2: Exploration to advanced multimodal generation.
 685 *arXiv preprint arXiv:2506.18871*, 2025.
- 686
- 687 Jinbo Xing, Menghan Xia, Yong Zhang, Haoxin Chen, Xintao Wang, Tien-Tsin Wong, and Ying
 688 Shan. DynamiCrafter: Animating Open-domain Images with Video Diffusion Priors. In *ECCV*,
 689 2024.
- 690
- 691 Jiaqi Xu, Xinyi Zou, Kunzhe Huang, Yunkuo Chen, Bo Liu, MengLi Cheng, Xing Shi, and Jun
 692 Huang. Easyanimate: A high-performance long video generation method based on transformer
 693 architecture. *arXiv preprint arXiv:2405.18991*, 2024.
- 694
- 695 Xing Yang, Yifan Zhu, Xingfei Liu, et al. Videograin: Modulating space-time attention for multi-
 696 grained video editing. In *arXiv preprint arXiv:2502.17258*, 2025.
- 697
- 698 Zhuoyi Yang, Jiayan Teng, Wendi Zheng, Ming Ding, Shiyu Huang, Jiazheng Xu, Yuanming Yang,
 699 Wenyi Hong, Xiaohan Zhang, Guanyu Feng, et al. Cogvideox: Text-to-video diffusion models
 700 with an expert transformer. *arXiv preprint arXiv:2408.06072*, 2024.
- 701
- 702 Yang Ye, Xianyi He, Zongjian Li, Bin Lin, Shenghai Yuan, Zhiyuan Yan, Bohan Hou, and Li Yuan.
 703 Imgedit: A unified image editing dataset and benchmark. *arXiv preprint arXiv:2505.20275*, 2025.
- 704
- 705 Yan Zeng, Guoqiang Wei, Jian Zheng, Jiaxin Zou, Yang Wei, Yuchen Zhang, and Hang Li. Make
 706 Pixels Dance: High-Dynamic Video Generation. In *CVPR*, 2024.
- 707
- 708 Lvmin Zhang and Maneesh Agrawala. Packing input frame context in next-frame prediction models
 709 for video generation. *arXiv preprint arXiv:2504.12626*, 2025.

702 Shiwei Zhang, Jiayu Wang, Yingya Zhang, Kang Zhao, Hangjie Yuan, Zhiwu Qin, Xiang Wang,
703 Deli Zhao, and Jingren Zhou. I2VGen-XL: High-Quality Image-to-Video Synthesis via Cascaded
704 Diffusion Models. *arXiv preprint arXiv:2311.04145*, 2023.

705
706 Zhongwei Zhang, Fuchen Long, Zhaofan Qiu, Yingwei Pan, Wu Liu, Ting Yao, and Tao Mei.
707 Motionpro: A precise motion controller for image-to-video generation, 2025. URL <https://arxiv.org/abs/2505.20287>.

708
709 Dian Zheng, Ziqi Huang, Hongbo Liu, Kai Zou, Yinan He, Fan Zhang, Yuanhan Zhang, Jingwen He,
710 Wei-Shi Zheng, Yu Qiao, and Ziwei Liu. Vbench-2.0: Advancing video generation benchmark
711 suite for intrinsic faithfulness, 2025. URL <https://arxiv.org/abs/2503.21755>.

712

713

714

715

716

717

718

719

720

721

722

723

724

725

726

727

728

729

730

731

732

733

734

735

736

737

738

739

740

741

742

743

744

745

746

747

748

749

750

751

752

753

754

755

756	APPENDIX CONTENTS	
757		
758		
759	A The Use of Large Language Models	16
760		
761	B Detailed Proofs for Attention Scaling Analysis	16
762	B.1 Lemma 1: Q/K Scaling as Temperature Control	16
763	B.2 Lemma 2: Entropy Monotonicity Under Scaling	16
764	B.3 Theorem: Asymptotic Curvature Decay Under Scaling	17
765		
766		
767	C Theoretical Guarantees of Attention Scaling	17
768		
769	C.1 Lipschitz Continuity of Attention Output	17
770	C.2 Impact on a Single Diffusion Step	18
771		
772	D Details of OmitI2V Benchmark	19
773		
774	D.1 Statistical Analysis	19
775	D.2 Qualitative Visualization of Samples	20
776		
777	E Details about Baseline	21
778		
779		
780	F Implementation Details	28
781	F.1 Attention Scaling Modulation.	28
782	F.2 Implementation Details of Block-Level Foreground Analysis	28
783	F.3 Implementation Details of Step-Level Scheduling	28
784	F.4 Pseudo-code.	29
785		
786		
787	G Discussion	29
788		
789	G.1 Exploring the Effect of Different Blur Levels on Generation Results	29
790	G.2 Ablation on the Scaling Coefficient	30
791	G.3 Inference Efficiency	31
792	G.4 Results on Other I2V Benchmarks	31
793	G.5 Validating Semantic Fidelity Metrics with Human Evaluation	32
794	G.6 Analysis of the VQA-based Semantic Evaluator on OmitI2V	33
795		
796		
797		
798	H Qualitative Visualization of Evaluation Results	34
799		
800		
801		
802		
803		
804		
805		
806		
807		
808		
809		

810 A THE USE OF LARGE LANGUAGE MODELS

811
 812 Large language models (LLMs) (Hurst et al., 2024) are used as general-purpose assistants for lan-
 813 guage polishing (grammar, tone), LaTeX phrasing, and minor reorganization of exposition. LLMs
 814 are *not* used to design experiments, generate or label data, or produce claims. The authors take full
 815 responsibility for all content.

816 817 B DETAILED PROOFS FOR ATTENTION SCALING ANALYSIS

818 B.1 LEMMA 1: Q/K SCALING AS TEMPERATURE CONTROL

819
 820 **Statement.** Let $Q'_t = \gamma_t Q_t$ and $K'_t = \eta_t K_t$. Then

$$821 \quad 822 \quad 823 \quad Z'_t = \frac{1}{\sqrt{d}} Q'_t K'^\top = (\gamma_t \eta_t) Z_t := \alpha_t Z_t, \quad (17)$$

824
 825 so for the i -th row the attention is $p^{(i)}(\alpha_t) = \sigma(\alpha_t z_t^{(i)})$, i.e., a row-wise softmax with inverse
 826 temperature α_t . In particular, scaling only Q (resp. K) yields $\alpha_t = \gamma_t$ (resp. $\alpha_t = \eta_t$).

827
 828 **Proof.** By definition,

$$829 \quad 830 \quad Z_t = \frac{1}{\sqrt{d}} Q_t K_t^\top, \quad (18)$$

831 and after scaling,

$$832 \quad 833 \quad Z'_t = \frac{1}{\sqrt{d}} (\gamma_t Q_t) (\eta_t K_t)^\top = (\gamma_t \eta_t) Z_t. \quad (19)$$

834 For the i -th row,

$$835 \quad 836 \quad \sigma(\alpha_t z_t^{(i)})_j = \frac{\exp(\alpha_t z_{t,j}^{(i)})}{\sum_{k=1}^m \exp(\alpha_t z_{t,k}^{(i)})}, \quad (20)$$

837 which is softmax with inverse temperature α_t (temperature $T = 1/\alpha_t$). \square

838 B.2 LEMMA 2: ENTROPY MONOTONICITY UNDER SCALING

839
 840 **Statement.** For any query i and $\alpha > 0$,

$$841 \quad 842 \quad \frac{d}{d\alpha} H_i(\alpha) = -\alpha \text{Var}_{p^{(i)}(\alpha)}[z^{(i)}] \leq 0. \quad (21)$$

843
 844 **Proof.** Let

$$845 \quad 846 \quad p_j^{(i)}(\alpha) = \frac{e^{\alpha z_j^{(i)}}}{\sum_k e^{\alpha z_k^{(i)}}}, \quad (22)$$

847 and write the entropy as

$$848 \quad 849 \quad H_i(\alpha) = \log \sum_j e^{\alpha z_j^{(i)}} - \alpha \sum_j p_j^{(i)}(\alpha) z_j^{(i)}. \quad (23)$$

850 Define $\mu(\alpha) = \sum_j p_j^{(i)}(\alpha) z_j^{(i)} = \mathbb{E}_{p^{(i)}(\alpha)}[z^{(i)}]$. Then

$$851 \quad 852 \quad \frac{d}{d\alpha} \log \sum_j e^{\alpha z_j^{(i)}} = \frac{\sum_j z_j^{(i)} e^{\alpha z_j^{(i)}}}{\sum_k e^{\alpha z_k^{(i)}}} = \mu(\alpha). \quad (24)$$

853 Using $\frac{\partial p_j}{\partial \alpha} = p_j(z_j^{(i)} - \mu(\alpha))$,

$$854 \quad 855 \quad \frac{d}{d\alpha} \mu(\alpha) = \sum_j z_j^{(i)} \frac{\partial p_j}{\partial \alpha} = \sum_j z_j^{(i)} p_j(z_j^{(i)} - \mu(\alpha)) = \mathbb{E}_p[z^{(i)}]^2 - \mu(\alpha)^2 = \text{Var}_p[z^{(i)}]. \quad (25)$$

856
 857 Therefore,

$$858 \quad 859 \quad \frac{d}{d\alpha} H_i(\alpha) = \mu(\alpha) - \left(\mu(\alpha) + \alpha \text{Var}_p[z^{(i)}] \right) = -\alpha \text{Var}_p[z^{(i)}] \leq 0. \quad (26)$$

860 Equality holds iff the row logits are degenerate (zero variance). \square

864 B.3 THEOREM: ASYMPTOTIC CURVATURE DECAY UNDER SCALING
865866 **Statement.** Let $p^{(i)}(\alpha) = \sigma(\alpha z^{(i)})$ and

867
$$868 H_i(\alpha) = \nabla_{z^{(i)}}^2 \Phi(\alpha z^{(i)}) = \alpha^2 \left(\text{Diag}(p^{(i)}(\alpha)) - p^{(i)}(\alpha) p^{(i)}(\alpha)^\top \right). \quad (27)$$

869

870 Let $j^* = \arg \max_j z_j^{(i)}$ and $\Delta_i = z_{j^*}^{(i)} - \max_{j \neq j^*} z_j^{(i)} > 0$. Then there exists $\alpha_* = \alpha_*(\Delta_i, m)$ such
871 that for all $\alpha \geq \alpha_*$,

872
$$\frac{d}{d\alpha} \|H_i(\alpha)\|_{\text{spec}} \leq 0, \quad \lim_{\alpha \rightarrow \infty} \|H_i(\alpha)\|_{\text{spec}} = 0. \quad (28)$$

873

874 **Proof.** First, a standard softmax gap bound gives

875
$$876 p_{j^*} = \frac{1}{1 + \sum_{j \neq j^*} \exp(\alpha(z_j^{(i)} - z_{j^*}^{(i)}))} \geq \frac{1}{1 + (m-1)e^{-\alpha\Delta_i}}, \quad (29)$$

877

878 hence, for the tail mass $\varepsilon(\alpha) := 1 - p_{j^*}$,

879
$$880 \varepsilon(\alpha) \leq \frac{(m-1)e^{-\alpha\Delta_i}}{1 + (m-1)e^{-\alpha\Delta_i}} \leq (m-1)e^{-\alpha\Delta_i}. \quad (30)$$

881

882 Let $C(p) = \text{Diag}(p) - pp^\top$ so that $H_i(\alpha) = \alpha^2 C(p)$. For any i , $C_{ii} = p_i(1-p_i)$ and $C_{ij} = -p_i p_j$
883 for $i \neq j$. By the Gershgorin disk theorem, every eigenvalue λ satisfies
884

885
$$\lambda \leq \max_i \{C_{ii} + \sum_{j \neq i} |C_{ij}|\} = \max_i \{2p_i(1-p_i)\}. \quad (31)$$

886

887 When α is large, $p_{j^*} = 1 - \varepsilon(\alpha)$ and $\sum_{j \neq j^*} p_j = \varepsilon(\alpha)$, so

888
$$889 \max_i p_i(1-p_i) = \max_i \{(1-\varepsilon)\varepsilon, \max_{j \neq j^*} p_j(1-p_j)\} \leq \varepsilon(\alpha). \quad (32)$$

890

891 Therefore,

892
$$\|C(p)\|_{\text{spec}} \leq 2\varepsilon(\alpha), \quad \|H_i(\alpha)\|_{\text{spec}} \leq 2\alpha^2(m-1)e^{-\alpha\Delta_i}. \quad (33)$$

893

894 The right-hand side tends to 0 as $\alpha \rightarrow \infty$, proving the limit. Moreover,

895
$$896 \frac{d}{d\alpha} (\alpha^2 e^{-\alpha\Delta_i}) = \alpha e^{-\alpha\Delta_i} (2 - \alpha\Delta_i), \quad (34)$$

897

898 which is nonpositive for $\alpha \geq 2/\Delta_i$. Hence there exists $\alpha_* = \alpha_*(\Delta_i, m)$ (e.g., $\alpha_* \geq 2/\Delta_i$) such
899 that $\|H_i(\alpha)\|_{\text{spec}}$ is eventually nonincreasing. \square 900 **Intuition.** As α grows, softmax mass collapses onto the top logit. The tail mass decays exponentially in $\alpha\Delta_i$, forcing the non-principal directions to vanish. Although the prefactor α^2 can
901 initially increase curvature, the exponential tail dominates asymptotically, so the spectral norm ultimately decreases and converges to zero.905 C THEORETICAL GUARANTEES OF ATTENTION SCALING
906

907 C.1 LIPSCHITZ CONTINUITY OF ATTENTION OUTPUT

908 We consider the attention output for query i under Q/K scaling factor α :

909
$$910 y^{(i)}(\alpha) = \sum_{j=1}^m p_j^{(i)}(\alpha) V_j = V^\top p^{(i)}(\alpha), \quad (35)$$

911

912 where $p^{(i)}(\alpha) = \text{softmax}(\alpha z^{(i)})$.913 **Theorem C.1** (Lipschitz Continuity of Attention Output). *For any $\alpha_1, \alpha_2 > 0$, the following bound
914 holds:*

915
$$916 \|y^{(i)}(\alpha_1) - y^{(i)}(\alpha_2)\|_2 \leq \frac{1}{2} \|V\|_2 \|z^{(i)}\|_2 |\alpha_1 - \alpha_2|. \quad (36)$$

917

918 *Detailed Proof.* The derivative of $y^{(i)}(\alpha)$ w.r.t. α is
 919

$$920 \quad \frac{d}{d\alpha} y^{(i)}(\alpha) = V^\top \frac{d}{d\alpha} p^{(i)}(\alpha). \quad (37)$$

922 The softmax Jacobian is
 923

$$924 \quad \frac{\partial p_j^{(i)}}{\partial \alpha} = p_j^{(i)} \left(z_j^{(i)} - \sum_k p_k^{(i)} z_k^{(i)} \right) = p_j^{(i)} (z_j^{(i)} - \mathbb{E}_{p^{(i)}}[z^{(i)}]). \quad (38)$$

928 Hence, in vector form:
 929

$$930 \quad \frac{d}{d\alpha} p^{(i)}(\alpha) = \text{Diag}(p^{(i)}) z^{(i)} - (p^{(i)} z^{(i)\top}) p^{(i)}. \quad (39)$$

932 It is known that the spectral norm of this softmax derivative is bounded by
 933

$$934 \quad \left\| \frac{d}{d\alpha} p^{(i)}(\alpha) \right\|_2 \leq \frac{1}{2} \|z^{(i)}\|_2. \quad (40)$$

936 Finally,
 937

$$938 \quad \left\| \frac{d}{d\alpha} y^{(i)}(\alpha) \right\|_2 \leq \|V\|_2 \left\| \frac{d}{d\alpha} p^{(i)}(\alpha) \right\|_2 \leq \frac{1}{2} \|V\|_2 \|z^{(i)}\|_2. \quad (41)$$

940 By the mean value theorem,
 941

$$942 \quad \|y^{(i)}(\alpha_1) - y^{(i)}(\alpha_2)\|_2 \leq \frac{1}{2} \|V\|_2 \|z^{(i)}\|_2 |\alpha_1 - \alpha_2|, \quad (42)$$

944 proving Lipschitz continuity. \square
 945

946 **Remark.** This theorem guarantees that scaling Q/K with α produces a bounded change in attention
 947 outputs, proportional to the magnitude of α deviation.
 948

949 C.2 IMPACT ON A SINGLE DIFFUSION STEP

950 Consider a single DDIM/ODE update:
 951

$$952 \quad x_{t-1} = a_t x_t + b_t \varepsilon_\theta(x_t, t), \quad (43)$$

954 where ε_θ is L_y -Lipschitz in the attention output y .
 955

956 **Proposition C.2** (Upper Bound on State Deviation). *If selective Q/K scaling is applied at step t
 957 with factor α_t , then the updated state deviation satisfies*

$$958 \quad \|x'_{t-1} - x_{t-1}\|_2 \leq |b_t| L_y \cdot \frac{1}{2} \|V_t\|_2 \|z_t^{(i)}\|_2 |\alpha_t - 1|. \quad (44)$$

960 *Detailed Proof.* Let ε'_θ denote the modified noise prediction after scaling. By Lipschitz continuity:
 961

$$962 \quad \|\varepsilon'_\theta - \varepsilon_\theta\|_2 \leq L_y \|y' - y\|_2 \leq L_y \cdot \frac{1}{2} \|V_t\|_2 \|z_t^{(i)}\|_2 |\alpha_t - 1|. \quad (45)$$

964 The diffusion step multiplies this perturbation by b_t :
 965

$$966 \quad \|x'_{t-1} - x_{t-1}\|_2 = |b_t| \|\varepsilon'_\theta - \varepsilon_\theta\|_2 \leq |b_t| L_y \cdot \frac{1}{2} \|V_t\|_2 \|z_t^{(i)}\|_2 |\alpha_t - 1|, \quad (46)$$

969 proving the proposition. \square
 970

971 **Remark.** This bound ensures that selective attention scaling introduces controlled perturbations,
 972 allowing smooth adjustment of semantic fidelity without destabilizing the generation process.
 973

972 **D DETAILS OF OMITI2V BENCHMARK**
973974 OmitI2V is a benchmark designed to assess the capability of generating videos from images driven
975 by textual instructions, specifically within complex scenarios. Unlike traditional image-to-video
976 tasks, our focus is more on “editing” than “generation”. Given an image and a natural language
977 instruction, the model outputs a video that accurately performs the specified *additions, deletions, or*
978 *modifications*, while preserving the identity, structure, and physical consistency.979 **Task Definition.** 1) **Operation Types:** Covering Addition, Deletion, and Modification, representing
980 the most common human interventions in visual media. 2) **Granularity Requirements:** We specify
981 extensible subtypes, ensuring tasks are both diagnostic and diverse. This fine granularity allows for
982 a comprehensive assessment across multiple dimensions.
983984 **Data Construction.** The dataset combines both real and synthetic data: 1) **Source Images:** Selected
985 open image or video dataset to ensure high resolution and clear copyright. 2) **Synthetic Enhancement:**
986 Using GPT-4o to generate rare and extreme scenarios (e.g., severe weather, sci-fi effects) to
987 broaden distribution coverage. 3) **Manual Curation and Annotation:** Image-instruction pairs are
988 designed and curated by humans to ensure clear intent.
989990 **Evaluation Methodology.** For evaluating, we employ existing metrics, such as dynamic degree
991 and aesthetic quality in Vbench (Huang et al., 2024), to assess the quality of generated videos.
992 Notably, we do not calculate subject consistency and background consistency, given the nature of
993 adding or removing subjects. Additionally, we introduce Visual Question Answering (VQA), where
994 a Multimodal Large Language Model (MLLM) answers questions based on video content, thereby
995 enhancing the comprehensiveness of the evaluation.
996997 **Attention Analysis in Generative Models.** Attention-based modulation has attracted increasing
998 interest as a method to enable zero-shot image and video editing (Liu et al., 2024a). For image
999 editing, prior work manipulates distinct components of the attention mechanism (Hertz et al., 2022;
1000 Cao et al., 2023) to regulate text-image correspondence while preserving geometric and structural
1001 properties of the source content (Liu et al., 2024a; Chen et al., 2024). In the video setting, these ideas
1002 are extended to enforce temporal consistency across frames: recent methods adapt cross-attention
1003 for sequence-level control (Qi et al., 2023; Cai et al., 2025; Jin et al., 2025; Yang et al., 2025) or
1004 integrate self-attention with masks derived from cross-attention features (Liu et al., 2024b; Ma et al.,
1005 2025) to steer the generative process. In this work, we examine TI2V prompt adherence from an
1006 energy-based perspective and empirically establish a connection between attention distribution and
1007 semantic fidelity: lower attention entropy is associated with stronger semantic alignment.
10081009 **D.1 STATISTICAL ANALYSIS**
10101011 Figure 4 summarizes the composition of the OmitI2V benchmark across three axes: edit type, visual
1012 domain, and image source. These statistics indicate that the benchmark is well-balanced along the
1013 primary task dimension and encompasses a broad spectrum of real-world and synthetic content.
10141015 **Edit-type balance.** We enforce near-uniform sampling across the three core types. *Modification*
1016 tasks constitute 34.19%, *Addition* tasks 33.16%, and *Deletion* tasks 32.65%. This equilibrium pre-
1017 vents any single operation from dominating the evaluation signal and enables fair comparisons.
10181019 **Domain diversity.** We annotate every sample with a fine-grained domain label drawn from the
1020 eight mutually-exclusive classes defined below. These labels capture both semantic content and
1021 context, enabling granular diagnostics of model robustness. **Living Beings** Any depiction of bio-
1022 logical organisms, including but not limited to humans (portraits, crowd scenes, daily activities),
1023 domestic and wild animals, and anthropomorphic creatures. The defining criterion is the presence
1024 of animate life as the primary subject. **Arts & Entertainment** Creative or performative artifacts
1025 that are either hand-drawn or computer-generated, such as cartoons, anime, video-game assets, CGI
sequences, virtual idols, and stylized artistic renditions. Realistic photographs of artworks in situ
are excluded. **Nature & Environment** Representations of the natural world, spanning landscapes,
1026 seascapes, forests, deserts, weather phenomena, macro flora, and non-anthropocentric fauna in their
1027 ecological context. Urban parks are classified here only when the natural element dominates the
1028 composition. **Structures** Man-made architectural entities, from iconic landmarks and historical ed-
1029 ifices to vernacular housing and industrial facilities. Interior shots are included when architectural
1030

design is the focal element. **Objects**) Inanimate physical items, ranging from everyday household articles and consumer products to vehicles, tools, and brand logos. Items are labeled OBJ when they constitute the primary subject rather than mere scene fillers. **Technological & Virtual Elements** Artifacts of modern technology and digital culture, including user-interface screenshots, HUD overlays, AR/VR visualizations, holographic projections, and abstract algorithmic renderings. **Food & Necessities** Edible goods, beverages, cooking processes, and essential daily commodities. Prepared dishes, raw ingredients, and packaged products are all subsumed under this class. **Text & Communication** Static or dynamic textual content designed for human communication, such as signage and logos, provided that text is the dominant visual element.

Provenance breakdown. Real photographs dominate the collection (75.58%). Animation frames contribute 18.25%, and purely synthetic images rendered or hallucinated by GPT-4o make up 4.63%. This mix exposes models to both natural statistics and out-of-distribution, synthetic edge cases.

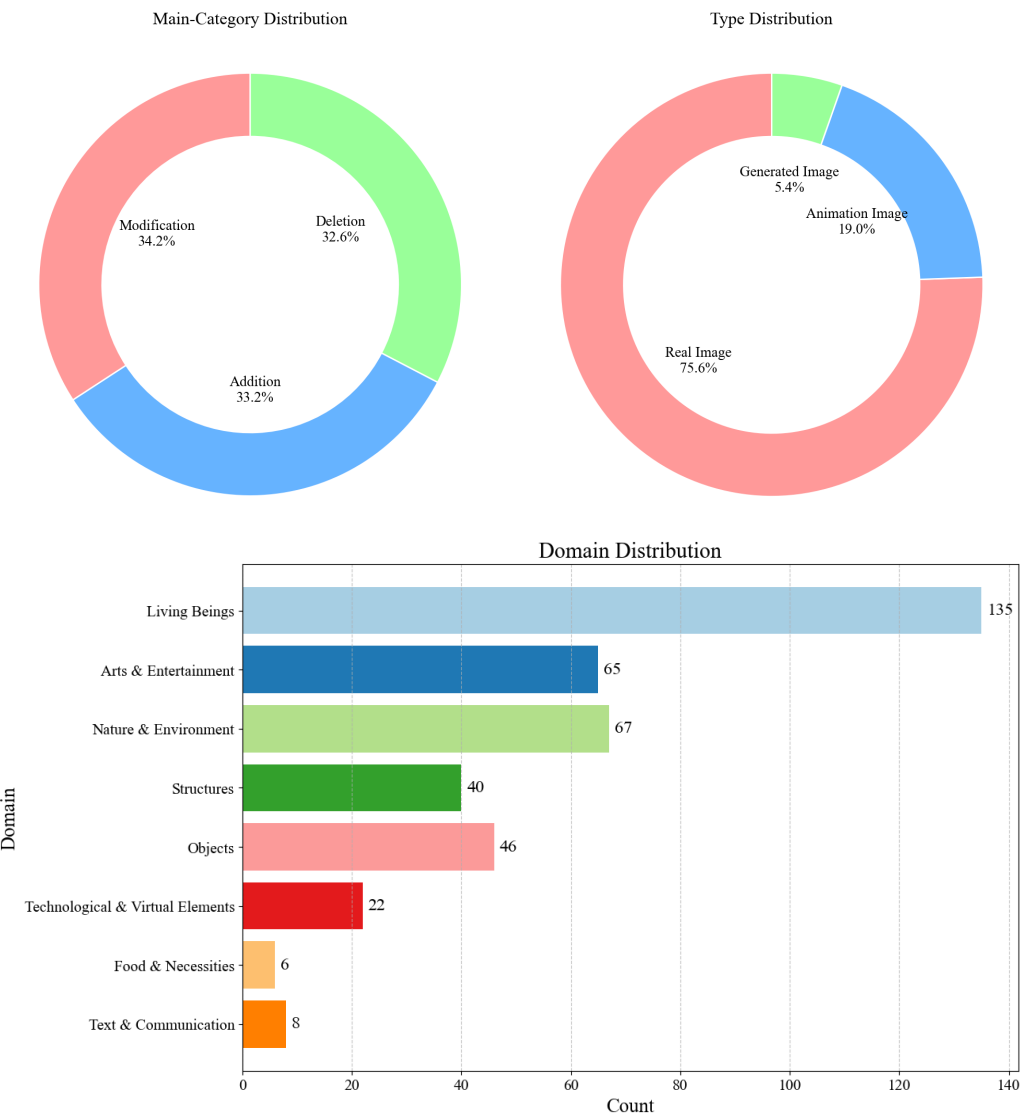


Figure 4: Statistical distributions of the OmitI2V benchmark.

D.2 QUALITATIVE VISUALIZATION OF SAMPLES

In this section, we delve into the qualitative visualization of the samples (Figure 5-Figure 10). The description of each sample contains clear expected changes and key elements. This information not

1080 only aids in understanding the content depicted in the images but also highlights the critical points
 1081 of change within the visualization. This interpretive approach ensures the uniformity and accuracy
 1082 of the sample presentation, allowing each representative change to clearly convey its core concept.
 1083

1084 Additionally, the samples are categorized into different main and sub-categories. This organizational
 1085 method enables a systematic approach to browsing and analyzing the samples. For specific domains,
 1086 such as human, nature, or animation, this categorization helps us pinpoint and comprehend factors
 1087 that affect particular types of images.

1088 The questions and answers in the samples further explore various aspects of the images, ranging from
 1089 action correctness to object presence and dynamic changes. These questions assist in evaluating
 1090 the standards of the images and their transformations, allowing observers to analyze the sample
 1091 performance from an evaluative perspective.

1092 E DETAILS ABOUT BASELINE

1093 We select **FramePack** and **Wan2.1** as baselines to cover the two dominant architectural lineages in
 1094 current diffusion-based video models.

1095 **MM-DiT family.** FramePack instantiates the MM-DiT architecture, which interleaves multi-modal
 1096 (text–image–video) tokens within a single transformer. Beyond state-of-the-art short-form editing
 1097 quality, FramePack uniquely supports autoregressive long-video generation; this capability is essen-
 1098 tial for stress-testing temporal coherence when edits propagate over extended horizons.

1099 **DiT family.** Wan2.1 adopts the standard DiT backbone that factorizes spatial and temporal attention.
 1100 Its simplicity, parameter efficiency, and widespread adoption make it a representative baseline for the
 1101 DiT lineage. Together, these two models span the principal design choices—joint versus factorized
 1102 attention, short versus autoregressive generation—thereby establishing a rigorous and reproducible
 1103 reference for OmitI2V evaluations.

1104

1105

1106

1107

1108

1109

1110

1111

1112

1113

1114

1115

1116

1117

1118

1119

1120

1121

1122

1123

1124

1125

1126

1127

1128

1129

1130

1131

1132

1133

1134
 1135
 1136
 1137
 1138
 1139
 1140
 1141
 1142
 1143
 1144
 1145
 1146
 1147
 1148
 1149
 1150
 1151
 1152
 1153
 1154
 1155
 1156
 1157



1158
 1159
 1160
 1161
 1162
 1163
 1164
 1165
 1166
 1167
 1168
 1169
 1170

JSON Sample

ID: sample_0
Image-path: OmitI2V/modification/pose/human/1.jpg
Prompt: The guy pushes out the ball with superpower.
Expected change: The man's pose changes to show him pushing the energy orb forward.
Key: man pushes an energy ball
Main Category: modification
Sub-category: pose
Domain: human
Type: generated image
Resolution: 1280x1280
Aspect Ratio: 1.0
Questions:

- Question:** Does the man's pose change to show him pushing forward?
Expected Answer: yes
Category: action correctness
- Question:** Does the energy orb move forward as the man pushes it?
Expected Answer: yes
Category: dynamic changes
- Question:** Is the man standing still throughout the video?
Expected Answer: no
Category: spatial relationship

1181
 1182
 1183
 1184
 1185
 1186
 1187

Figure 5: Sample (“Modification” task) from the OmitI2V benchmark.

1188
 1189
 1190
 1191
 1192
 1193
 1194
 1195
 1196
 1197
 1198
 1199
 1200
 1201
 1202
 1203
 1204



1205
 1206
 1207
 1208
 1209
 1210
 1211
 1212
 1213
 1214
 1215
 1216
 1217
 1218
 1219
 1220

JSON Sample

1221
 1222
 1223
 1224
 1225
 1226
 1227
 1228
 1229
 1230
 1231
 1232
 1233
 1234
 1235
 1236
 1237
 1238
 1239

ID: sample_118
Image-path: OmitI2V/modification/style/plant/2.jpg
Prompt: The sunflower field gradually shifts into an anime-style rendering, colors becoming more vibrant and outlines turning bold and stylized.

Expected change: The realistic sunflowers slowly transform into anime-style flowers with exaggerated textures, bright saturated colors, and defined outlines, while the background remains unchanged.

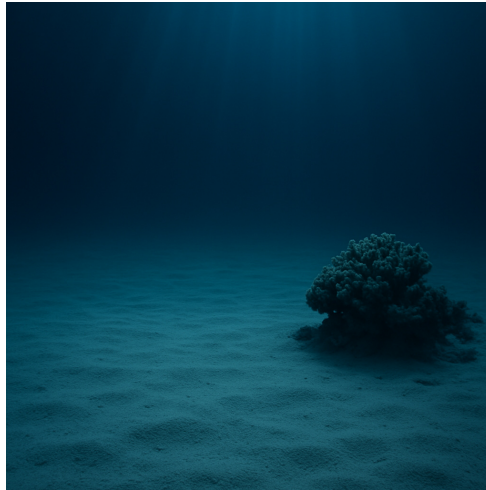
Key: sunflowers to anime style
Main Category: modification
Sub-category: style
Domain: plant
Type: real image
Change: yes
Resolution: 1920x1280
Aspect Ratio: 1.5
Questions:

- Question:** Do the sunflowers change into an anime style?
Expected Answer: yes
Category: dynamic changes
- Question:** Are the colors of the sunflowers more vibrant after the transformation?
Expected Answer: yes
Category: attribute accuracy
- Question:** Do the outlines of the sunflowers become less defined after the transformation?
Expected Answer: no
Category: attribute accuracy
- Question:** Do realistic textures on the sunflowers remain unchanged during the transformation?
Expected Answer: no
Category: attribute accuracy

1240
 1241

Figure 6: Sample (“Modification” task) from the OmitI2V benchmark.

1242
 1243
 1244
 1245
 1246
 1247
 1248
 1249
 1250
 1251
 1252
 1253
 1254
 1255
 1256
 1257
 1258
 1259



1260
 1261
 1262
 1263
 1264
 1265
 1266
 1267
 1268
 1269
 1270
 1271
 1272
 1273
 1274
 1275
 1276
 1277
 1278
 1279
 1280
 1281
 1282
 1283
 1284
 1285
 1286
 1287
 1288
 1289
 1290
 1291
 1292
 1293
 1294
 1295

JSON Sample

ID: sample_7
Image-path: OmitI2V/addition/appearance/animal/2.png
Prompt: Three small fish dart swiftly from the left side of the frame, swimming past vibrant coral and disappearing off to the right.
Expected change: Three small fish quickly appear from the left side of the screen and swim through the coral.
Key: Three small fish, swim quickly past, past the coral
Main Category: addition
Sub-category: appearance
Domain: animal
Type: generated image
Change: yes
Resolution: 1024x1024
Aspect Ratio: 1.0
Questions:

- Question:** Do the fish swim slowly past the coral?
Expected Answer: no
Category: action correctness
- Question:** Is the coral vibrant in color?
Expected Answer: yes
Category: attribute accuracy
- Question:** Do the fish appear from the right side of the frame?
Expected Answer: no
Category: spatial relationship
- Question:** Do the fish swim past the coral and then disappear off to the right?
Expected Answer: yes
Category: dynamic changes
- Question:** Are there more than three small fish in the video?
Expected Answer: no
Category: attribute accuracy

Figure 7: Sample (“Addition” task) from the OmitI2V benchmark.

1296
 1297
 1298
 1299
 1300
 1301
 1302
 1303
 1304
 1305
 1306
 1307
 1308
 1309
 1310
 1311
 1312
 1313



1314
 1315
 1316
 1317
 1318
 1319
 1320
 1321
 1322
 1323
 1324
 1325
 1326
 1327
 1328
 1329
 1330
 1331
 1332
 1333
 1334
 1335
 1336
 1337
 1338
 1339
 1340
 1341
 1342
 1343
 1344
 1345
 1346
 1347
 1348
 1349

JSON Sample

ID: sample_118
Image-path: OmitI2V/addition/object/plant/1.jpg
Prompt: A cactus suddenly sprouts and grows tall next to the mushroom, its spines and green stems appearing as it rises from the ground.
Expected change: A cactus suddenly sprouts beside the mushroom, growing taller with its spines and green stems clearly forming as it emerges from the ground.
Key: cactus grows, next to mushroom
Main Category: addition
Sub-category: object
Domain: plant
Type: real image
Change: yes
Resolution: 1024x1024
Aspect Ratio: 1.46
Questions:

- Question:** Does the cactus grow from the ground up in the video?
Expected Answer: no
Category: action correctness
- Question:** Is there a cactus growing next to a tree in the video?
Expected Answer: no
Category: attribute accuracy
- Question:** Does the mushroom grow taller than the cactus in the video?
Expected Answer: no
Category: attribute accuracy
- Question:** Do multiple cacti grow next to the mushroom in the video?
Expected Answer: yes
Category: object presence

Figure 8: Representative sample (“Addition” task) from the OmitI2V benchmark.

1350
 1351
 1352
 1353
 1354
 1355
 1356
 1357
 1358
 1359
 1360
 1361
 1362
 1363
 1364



1365
 1366
 1367
 1368
 1369
 1370
 1371
 1372
 1373
 1374
 1375
 1376
 1377
 1378
 1379
 1380
 1381
 1382
 1383
 1384
 1385
 1386
 1387
 1388
 1389
 1390
 1391
 1392
 1393
 1394
 1395
 1396
 1397
 1398
 1399
 1400
 1401
 1402
 1403

JSON Sample

ID: sample_112
Image-path: OmitI2V/deletion/vanish/nature/2.jpg
Prompt: The lush green mountain gradually erodes and disappears, leaving behind rolling sand dunes and a barren desert landscape.
Expected change: The green vegetation and rocky outcrops of the mountain fade away until only dunes of sand remain.
Key: mountain disappears, desert appears
Main Category: deletion
Sub-category: vanish
Domain: nature
Type: real image
Change: yes
Resolution: 1920x1280
Aspect Ratio: 1.5
Questions:

- Question:** Does the mountain remain visible throughout the video?
Expected Answer: no
Category: object presence
- Question:** Do sand dunes appear as the mountain erodes?
Expected Answer: yes
Category: action correctness
- Question:** Is the landscape at the end of the video primarily composed of lush green vegetation?
Expected Answer: no
Category: attribute accuracy
- Question:** Are there any rocky outcrops visible after the mountain has eroded?
Expected Answer: no
Category: object presence
- Question:** Does the desert landscape gradually form before the mountain disappears?
Expected Answer: yes
Category: dynamic changes

Figure 9: Sample (“Deletion” task) from the OmitI2V benchmark.

1404
1405
1406
1407
1408
1409
1410
1411
1412
1413
1414
1415
1416
1417
1418
1419
1420



1421
1422
1423
1424
1425
1426
1427
1428
1429
1430
1431
1432
1433
1434
1435
1436
1437
1438
1439
1440
1441
1442
1443
1444
1445
1446
1447
1448
1449
1450
1451
1452
1453
1454
1455
1456
1457

JSON Sample

ID: sample_121
Image-path: OmitI2V/deletion/vanish/human/2.jpg
Prompt: The woman gradually disappeared as she crouched down
Expected change: The woman gradually disappeared as she crouched down
Key: duck egg appears
Main Category: addition
Sub-category: object
Domain: human
Type: real image
Resolution: 1920x1280
Aspect Ratio: 1.5
Questions:

- Question:** Does the woman suddenly disappear?
Expected Answer: no
Category: action correctness
- Question:** Does the woman crouch down as she disappears?
Expected Answer: yes
Category: action correctness
- Question:** Is a duck egg visible in the scene at any point?
Expected Answer: yes
Category: object presence
- Question:** Does the woman's disappearance happen instantly without her crouching down?
Expected Answer: no
Category: dynamic changes
- Question:** Does the woman remain fully visible throughout the video?
Expected Answer: no
Category: dynamic changes

Figure 10: Sample (“Deletion” task) from the OmitI2V benchmark.

Model	Foreground-sensitive blocks
FramePack	$\{0, 2, 4, 5, 6, 7, 10, 11, 12, 13, 14, 15, 16, 17, 18, 19, 20, 21, 23, 25, 26, 27, 31, 33\}$
FramePack F1	$\{0, 1, 2, 3, 4, 5, 6, 7, 12, 13, 14, 15, 16, 18, 19, 20, 23, 25, 29, 32, 36, 37, 38, 39\}$
Wan2.1	$\{0, 2, 4, 5, 6, 7, 10, 11, 12, 13, 14, 15, 16, 17, 18, 19, 20, 21, 23, 25, 26, 27, 31, 33\}$

Table 10: **Foreground-sensitive block indices.** We report the blocks identified as foreground-sensitive for FramePack (single-block setting), FramePack-F1, and Wan2.1. These blocks are determined via the foreground ratio analysis described in Section F.2.

F IMPLEMENTATION DETAILS

F.1 ATTENTION SCALING MODULATION.

We implement both *scalar scaling* and *energy-based modulation* within the attention layers. For scalar scaling, a fixed coefficient $\gamma > 1$ is multiplied to either the query or key embeddings. For energy-based modulation, the scaling factor is adaptively computed from the attention logits via a monotonic function, strengthening focus when attention is diffuse.

F.2 IMPLEMENTATION DETAILS OF BLOCK-LEVEL FOREGROUND ANALYSIS

To examine how different transformer blocks distribute their focus between foreground and background, we conduct a block-level study on attention behavior in FramePack.

Token extraction. From each self-attention layer, we record the token representations $\mathbf{Z} \in \mathbb{R}^{B \times L \times D}$, where B is the batch size, L is the number of spatio-temporal tokens, and D is the embedding dimension. Tokens are grouped into T segments, each corresponding to a video frame. Frame-level attention scores are then obtained by row-wise summation of the attention matrix.

Foreground segmentation. To identify foreground regions, we use the latent noise estimate $\tilde{\epsilon} \in \mathbb{R}^{B \times D \times T \times H \times W}$. We apply PCA (Abdi & Williams, 2010) along the channel axis and retain the top three components, yielding pseudo-RGB projections. These projections are passed into SAM2 (Ravi et al., 2024) to generate binary masks that separate foreground from background.

Foreground ratio. Let $\mathbf{M} \in \mathbb{R}^{L \times L}$ denote the attention matrix of a block. For each token u , its aggregated attention score is defined as

$$s_u = \frac{1}{L} \sum_{v=1}^L M_{uv}. \quad (47)$$

Tokens with s_u larger than a preset threshold are regarded as high-attention tokens. The fraction of these tokens lying inside the foreground mask is defined as the *foreground ratio* $\rho^{(b)}$ for block b . A larger $\rho^{(b)}$ implies preference for foreground regions.

We average $\rho^{(b)}$ across 50 diverse prompts to obtain a stable estimate of each block’s attention bias. The results are in Table 10.

F.3 IMPLEMENTATION DETAILS OF STEP-LEVEL SCHEDULING

Step-level scheduling (SGS) activates modulation only within a predefined interval $[t_{\text{low}}, t_{\text{high}}]$ of the T -step denoising trajectory. In experiments, we instantiate three canonical windows corresponding to **early**, **middle**, and **late** phases:

$$m_{\text{early}}(t) = \mathbf{1}\left[\frac{t}{T} \in [0.00, 0.30]\right], \quad m_{\text{middle}}(t) = \mathbf{1}\left[\frac{t}{T} \in [0.35, 0.65]\right], \quad m_{\text{late}}(t) = \mathbf{1}\left[\frac{t}{T} \in [0.70, 1.00]\right].$$

These masks activate ASM over the first 30%, the central 30%, and the final 30% of steps, respectively; the remaining 10% serves as an inactive buffer to avoid boundary artifacts. Unless otherwise noted, we report results for all three schedules and an all-steps variant; based on ablations (Table ??), we adopt the *early-step* schedule as the default.

1512 **Algorithm 1:** Selective Scalar Scaling (with BGS and SGS)
1513
1514 **Input:** Query Q , Key K , Value V ; scaling factor $\gamma > 1$;
1515 step interval $[t_{\text{low}}, t_{\text{high}}]$; block threshold τ
1516 **Output:** Modulated attention output
1517 **for** each denoising step t **do**
1518 **if** $t \in [t_{\text{low}}, t_{\text{high}}]$ **then**
1519 // Step-level scheduling
1520 **for** each transformer block l **do**
1521 Compute foreground ratio $r^{(l)}$;
1522 **if** $r^{(l)} > \tau$ **then**
1523 // Block-level scheduling
1524 **if** modulate Query **then**
1525 $Q' \leftarrow \gamma \cdot Q$, $K' \leftarrow K$;
1526 **else if** modulate Key **then**
1527 $Q' \leftarrow Q$, $K' \leftarrow \gamma \cdot K$;
1528 Compute attention:
1529
$$\text{Attn}^{(l)} = \text{softmax}\left(\frac{Q'(K')^\top}{\sqrt{d_k}}\right) V$$

1530
1531

1532
1533 **Algorithm 2:** Selective Energy-based Modulation (with BGS and SGS)
1534
1535 **Input:** Query Q , Key K , Value V ; monotonic function $f(\cdot)$;
1536 step interval $[t_{\text{low}}, t_{\text{high}}]$; block threshold τ
1537 **Output:** Modulated attention output
1538 **for** each denoising step t **do**
1539 **if** $t \in [t_{\text{low}}, t_{\text{high}}]$ **then**
1540 **for** each transformer block l **do**
1541 Compute foreground ratio $r^{(l)}$;
1542 **if** $r^{(l)} > \tau$ **then**
1543 Compute logits $z = \frac{QK^\top}{\sqrt{d_k}}$;
1544 Compute adaptive scaling $\gamma = f(z)$ (Equation 10);
1545 Apply modulation: $K' \leftarrow \gamma \cdot K$ (or Q');
1546 Compute attention:
1547
$$\text{Attn}^{(l)} = \text{softmax}\left(\frac{Q'(K')^\top}{\sqrt{d_k}}\right) V$$

1548
1549

1550
1551 **F.4 PSEUDO-CODE.**

1552 The procedures are summarized in Algorithm 1 and Algorithm 2, which illustrate how block and
1553 step level scheduling are combined with scalar scaling or energy-based modulation.

1554
1555 **G DISCUSSION**

1556
1557 **G.1 EXPLORING THE EFFECT OF DIFFERENT BLUR LEVELS ON GENERATION RESULTS**

1558 To better understand the role of image perturbation, we vary the degree of Gaussian blur applied
1559 to the input image and analyze its effect on generation quality. As shown in Figure 11, increasing
1560 the blur level leads to stronger motion and more complex subject dynamics, but at the cost of de-
1561 graded visual fidelity. Conversely, mild blur provides a balanced improvement, enhancing semantic
1562 alignment while largely preserving perceptual quality. This highlights a trade-off between motion



Figure 11: Effect of varying Gaussian blur levels on I2V generation. Higher blur increases motion amplitude and subject complexity, but reduces visual fidelity. Mild blur improves semantic alignment while largely preserving perceptual quality.

richness and aesthetic sharpness, suggesting that blur can be interpreted as a controllable proxy for motion strength.

G.2 ABLATION ON THE SCALING COEFFICIENT

We also conduct ablation studies on the effect of the scaling coefficient applied in our guidance mechanism. The quantitative results are summarized in Figure 11. We observe a clear trend: as

Method	Semantic Alignment Evaluation			ViCLIP Score			Visual Quality Evaluation	
	Modification ↑	Addition ↑	Deletion ↑	Modification ↑	Addition ↑	Deletion ↑	Dynamic Degree ↑	Aesthetic Quality ↑
<i>FramePack</i>								
Original	64.99	68.55	58.14	20.83	21.08	20.43	20.05	63.94
Scalar scaling $\gamma = 1.25$	66.97	71.91	59.52	21.00	21.74	20.78	28.02	63.67
Scalar scaling $\gamma = 1.35$	67.15	73.44	59.86	21.38	22.03	21.05	28.28	63.41
<i>FramePack F1</i>								
Original	64.45	67.79	58.50	21.06	19.91	20.61	24.42	63.10
Scalar scaling $\gamma = 1.25$	68.04	70.21	60.12	21.75	20.57	20.92	32.68	62.12
Scalar scaling $\gamma = 1.35$	70.02	71.45	61.06	21.78	21.04	20.99	33.16	62.11

Table 11: Ablation about scaling coefficient.

Model	Runtime per video (s) ↓		Overhead (%) ↓
	Original	+Scalar	
FramePack	129.90	130.02	+0.09
FramePack F1	117.05	117.08	+0.03
Wan2.1	445.66	445.71	+0.01

Table 12: **Inference time comparison.** Our method introduces **negligible** inference overhead. Overhead is computed as $\frac{\text{Method} - \text{Original}}{\text{Original}} \times 100\%$. Experiments are conducted on a single NVIDIA H100 (80 GB). FramePack and FramePack-F1 generate 832×480 videos with 177 frames. Wan2.1 generates 800×480 videos with 81 frames.

the scaling coefficient increases, both semantic fidelity and dynamic degree consistently improve, indicating stronger alignment with the conditioning signal. However, this improvement comes at the cost of aesthetic quality, which degrades as the coefficient grows. This trade-off highlights the importance of choosing a moderate coefficient that balances semantic consistency with visual appeal. In practice, we select a coefficient that achieves a satisfactory compromise, ensuring faithful semantic control without overly sacrificing the overall aesthetics of the generated video.

G.3 INFERENCE EFFICIENCY

Our method selectively modulates attention only at foreground-sensitive blocks and within a limited interval of denoising steps; it is important to understand the impact on computational cost.

Let L denote the total number of transformer blocks and T the number of denoising steps. Suppose attention modulation is applied to $L_s \leq L$ blocks over $T_s \leq T$ steps. Then, the additional attention computation introduced by our scaling mechanism can be approximated as:

$$\Delta \text{FLOPs} \approx \frac{L_s}{L} \cdot \frac{T_s}{T} \cdot \text{FLOPs}_{\text{attn}}, \quad (48)$$

where $\text{FLOPs}_{\text{attn}}$ denotes the cost of a single attention operation in one block. This expression indicates that, by restricting modulation to a subset of blocks and steps, the computational overhead remains a small fraction of the total generation cost.

Empirically, as shown in Table 12, our method introduces only **negligible** inference overhead.

G.4 RESULTS ON OTHER I2V BENCHMARKS

To further validate the generalizability of our approach, we conduct experiments on the VBenchI2V benchmark. The results, summarized in Tables 13 - 14, show that our method consistently achieves higher average quality scores compared to the baselines. While the overall I2V score remains comparable to the baseline methods.

More specifically, when the scale coefficient is set below 1, all metrics except *Dynamic Degree* improve over the baseline. In contrast, when the coefficient is greater than 1, the *Dynamic Degree* metric increases significantly, while other indicators remain within a stable range. **This is analogous to the temperature parameter in large language models: by simply adjusting a single scale**

Metric	FramePack				
	Original	$\gamma = 0.95$	$\gamma = 1.15$	$\gamma = 1.25$	$\gamma = 1.35$
Video-Condition Dimension					
I2V subject	98.89	98.93	98.80	98.74	98.70
I2V background	99.01	99.02	98.96	99.15	99.01
Camera motion	61.21	60.81	61.73	61.47	60.63
Average I2V score	86.37	86.25	86.50	86.45	86.11
Video-Quality Dimension					
Subject consistency	96.53	96.65	96.13	95.89	95.58
Background consistency	97.88	97.83	97.78	98.22	97.75
Motion smoothness	99.53	99.54	99.50	99.48	99.45
Dynamic degree	28.86	26.02	32.93	35.77	38.61
Aesthetic quality	61.71	61.62	61.74	61.19	61.40
Imaging quality	70.62	70.70	70.44	70.23	70.45
Average quality score	75.86	75.39	76.42	76.80	77.21

Table 13: Ablation about scaling coefficient (Transposed).

Metric	FramePack F1				
	Original	$\gamma = 0.95$	$\gamma = 1.15$	$\gamma = 1.25$	$\gamma = 1.35$
Video-Condition Dimension					
I2V subject	98.88	98.91	98.68	98.63	98.58
I2V background	99.18	99.19	99.12	99.08	99.06
Camera motion	49.54	49.93	48.75	48.23	49.80
Average I2V score	82.53	82.68	82.18	81.98	82.48
Video-Quality Dimension					
Subject consistency	94.94	95.16	94.33	94.03	93.95
Background consistency	97.40	97.46	97.20	97.10	96.98
Motion smoothness	99.40	99.42	99.36	99.33	99.31
Dynamic degree	33.33	30.89	40.65	42.68	43.90
Aesthetic quality	61.25	61.29	61.10	61.06	60.97
Imaging quality	70.28	70.31	70.04	70.03	69.90
Average quality score	76.10	75.76	77.11	77.37	77.50

Table 14: Ablation about scaling coefficient (Transposed).

value, users can flexibly balance between aesthetic quality (smaller scale) and prompt fidelity (larger scale).

These results highlight the simplicity and effectiveness of our method. Without introducing additional training or complex modules, our approach provides a lightweight method for controlling video generation quality across diverse I2V benchmarks.

G.5 VALIDATING SEMANTIC FIDELITY METRICS WITH HUMAN EVALUATION

To validate the effectiveness of our metrics, we conduct a user study on a total of 60 samples, sampling 20 instances per semantic change type (*addition*, *deletion*, *modification*) with 5 people.

Setup. For each sample, we form a triplet: the original prompt and image, the video generated by a baseline model, and the video generated using our method. Human annotators rated each video along two dimensions: *semantic fidelity* and *aesthetic quality*, using a 1–7 Likert scale.

Method	Semantic Fidelity			Aesthetic Quality		
	Addition	Deletion	Modification	Addition	Deletion	Modification
Framepack	3.05	3.20	3.16	5.70	5.60	5.65
Framepack + Ours	5.72	5.80	5.82	5.63	5.56	5.63

Table 15: Human ratings (1–7 scale) for each semantic change type. Our metrics correlate well with human judgment across addition, deletion, and modification.

Results. Table 15 summarizes the average human scores compared with our OmitI2V metrics. We observe that the human ratings consistently align with the metric trends: videos generated with our method achieve higher semantic fidelity while maintaining comparable aesthetic quality.

G.6 ANALYSIS OF THE VQA-BASED SEMANTIC EVALUATOR ON OMITI2V

Our main semantic fidelity metric on OmitI2V is derived from a VQA model (Qwen2.5-VL-32B) answering yes/no questions about whether the requested edit has been correctly executed. Since this introduces a potential source of bias, we explicitly quantify its reliability and inspect its typical failure modes.

Quantitative error analysis. We manually annotated OmitI2V samples generated by FramePack V1 and computed False Positive (FP) and False Negative (FN) statistics for each edit type. Table 16 summarizes the error rates:

Main category	FP rate	FN rate	Overall error
Addition	0.78%	1.94%	2.71%
Deletion	0.92%	3.15%	4.07%
Modification	0.63%	2.76%	3.38%
All	0.77%	2.61%	3.38%

Table 16: Error statistics of the Qwen2.5-VL-32B evaluator on OmitI2V (FramePack V1). We report the FP rate, the FN rate, and overall error for each edit type.

The overall error remains around 3–4% across all three edit types, indicating that Qwen2.5-VL-32B is generally reliable as an automatic evaluator on this benchmark.

Observed systematic tendencies. When inspecting the incorrect cases, we observe two mild but interpretable tendencies:

- **False negatives on small or partially occluded objects (conservative behavior).** In some *addition* and *deletion* clips, the evaluator answers “no” to object-presence questions even though the target object is present but small, partially occluded, or overshadowed by a larger foreground object. A typical pattern is:

Question: “Is a cat visible in the video?”

Ground truth: Yes

Model answer: No, the video shows a bear walking through a valley, not a cat.

Here, the cat is indeed visible, but the evaluator attends mainly to the dominant animal and misses the smaller one, leading to a conservative negative prediction.

- **Over-endorsement of the prompt effect (slight positive bias).** In a few *modification* clips, the evaluator correctly detects that some visual change occurs, but overstates the strength of the edit. For example:

Question: “Does the instructor fade out of view while still holding the beaker?”

Ground truth: No

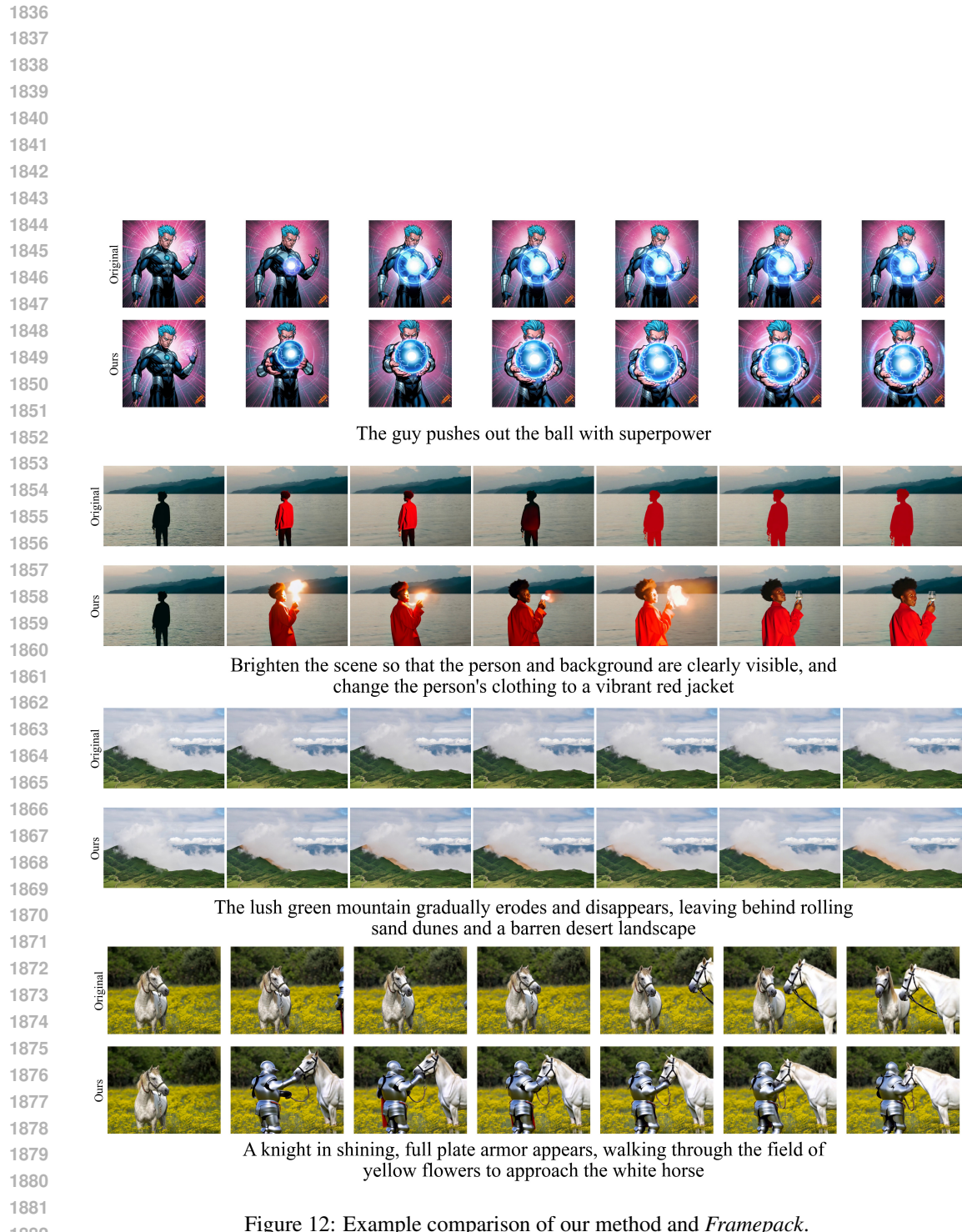
Model answer (abridged): Yes, the instructor gradually fades out of view while

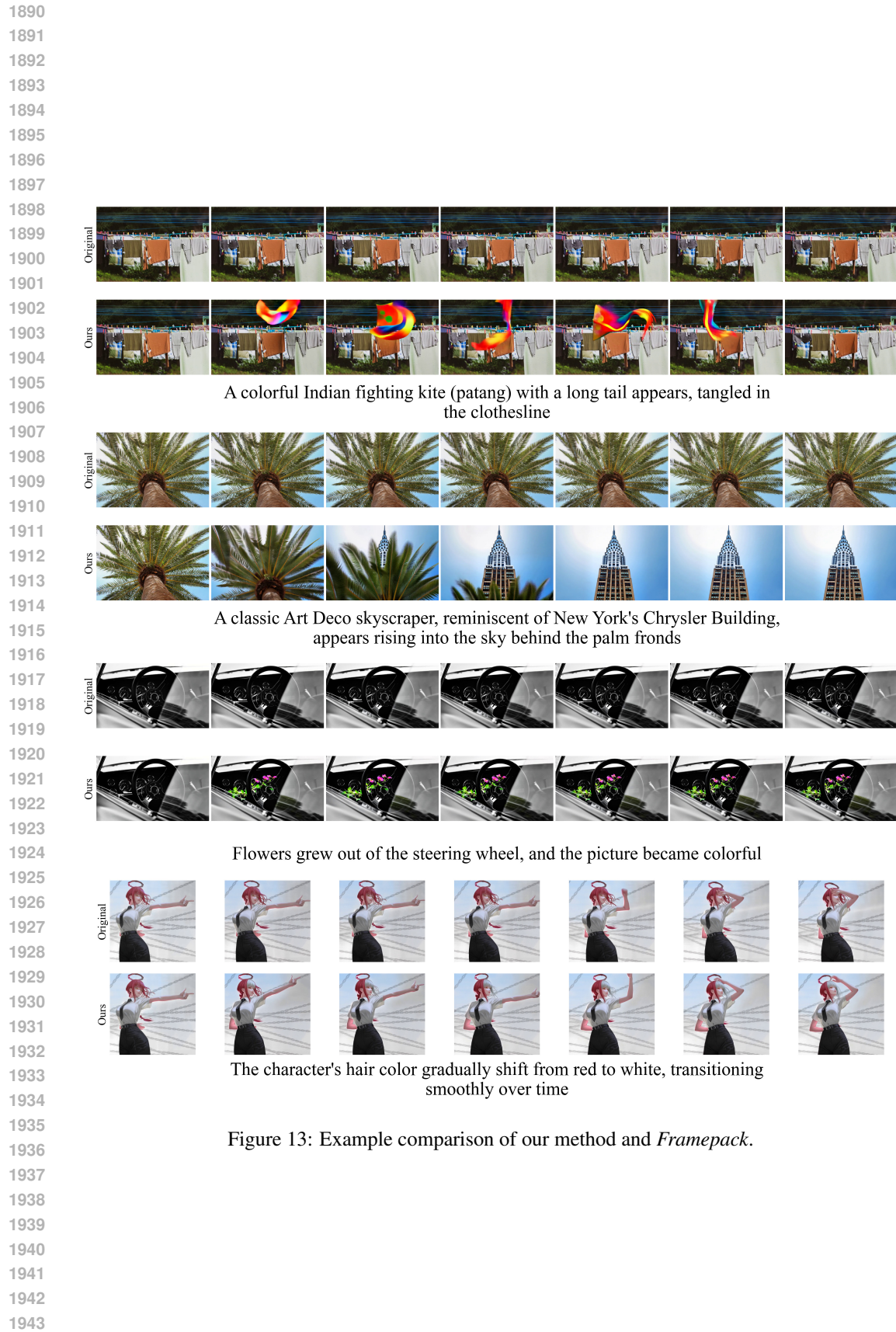
1782 still holding the beaker, indicating that their presence is being removed from the
1783 scene.
1784 Our frame-level inspection shows only mild transparency/compositing changes rather than
1785 a full fade-out. In such cases, the evaluator captures a real change but hallucinates a
1786 stronger, cleaner effect than what is actually rendered.
1787
1788 The identified failure cases mostly involve borderline or subtle situations (tiny objects, very mild
1789 appearance changes), whereas the majority of OmitI2V edits are clear semantic operations (adding,
1790 removing, or modifying an object), for which the evaluator behaves consistently.
1791

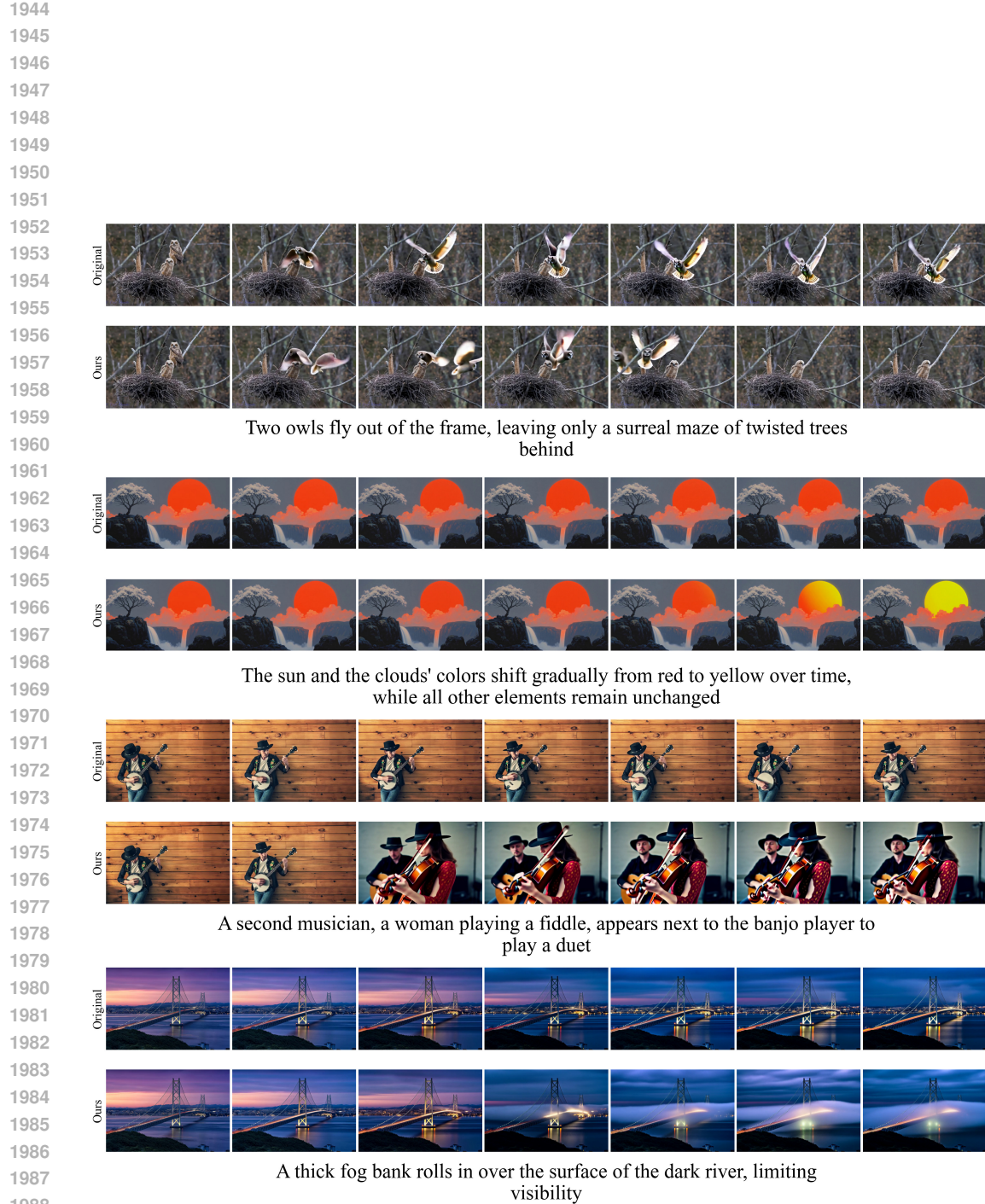
1792 H QUALITATIVE VISUALIZATION OF EVALUATION RESULTS

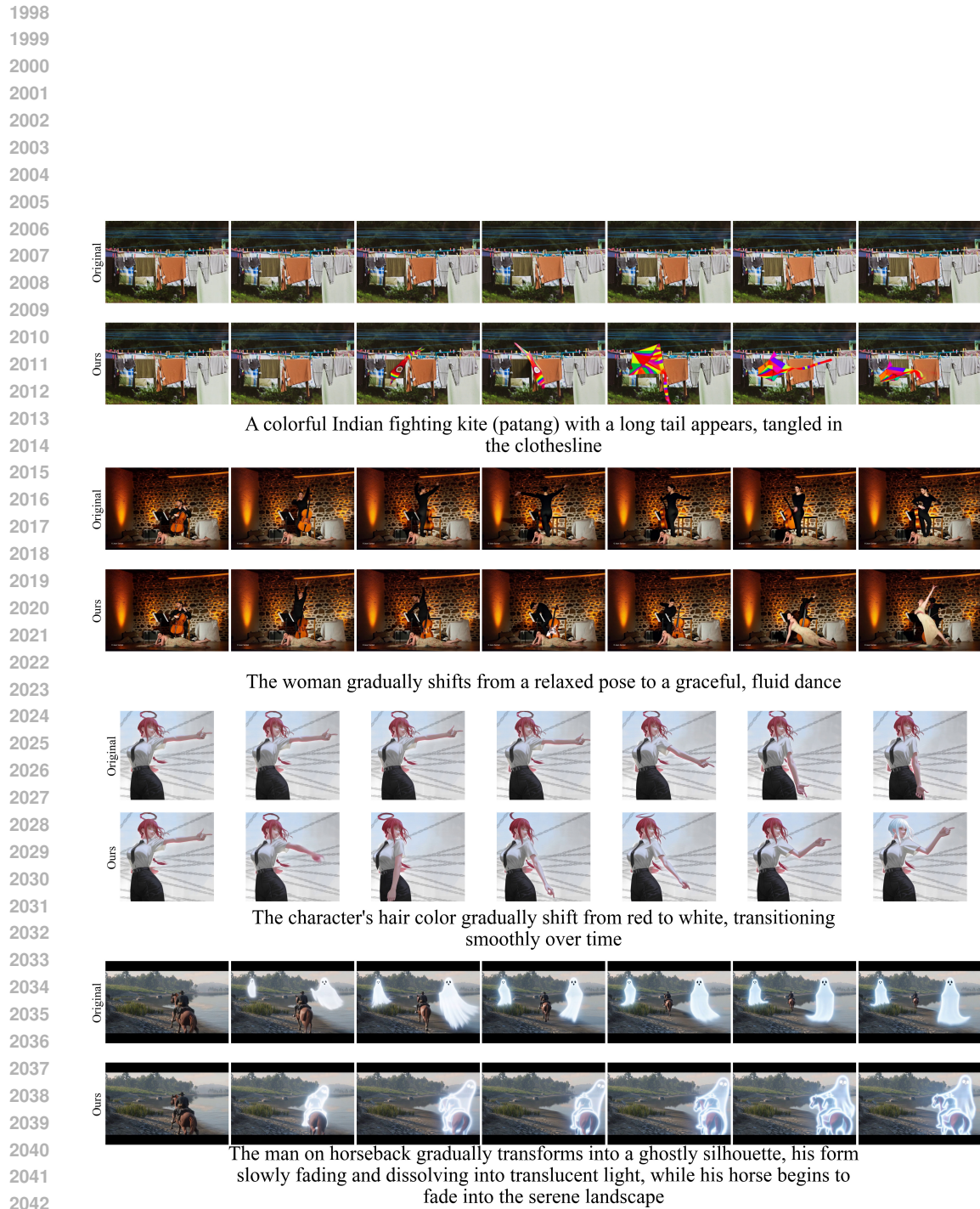
1793 To further demonstrate the effectiveness of our method, we provide qualitative visualizations com-
1794 paring the original videos, baseline methods (*Framepack*, *Framepack F1*, *Wan2.1*), and our ap-
1795 proach. These comparisons highlight improvements in both semantic consistency and visual qual-
1796 ity, showing that our method produces more faithful renderings with better alignment to the input
1797 prompts. Representative examples are presented in Figure 12 to Figure 17.
1798

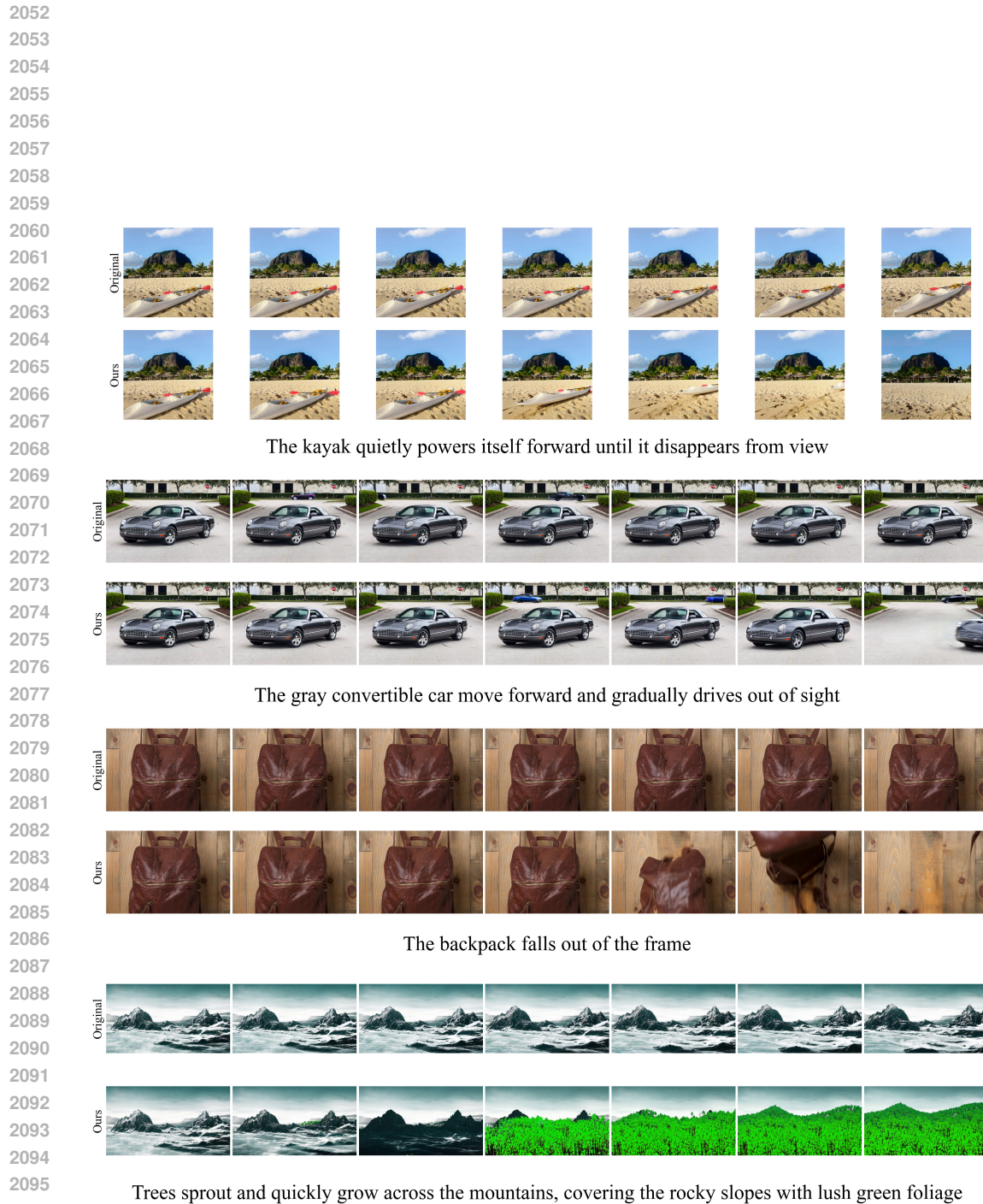
1799
1800
1801
1802
1803
1804
1805
1806
1807
1808
1809
1810
1811
1812
1813
1814
1815
1816
1817
1818
1819
1820
1821
1822
1823
1824
1825
1826
1827
1828
1829
1830
1831
1832
1833
1834
1835

Figure 12: Example comparison of our method and *Framepack*.

Figure 13: Example comparison of our method and *Framepack*.

Figure 14: Example comparison of our method and *Framepack F1*.

Figure 15: Example comparison of our method and *Framepack F1*.

Figure 16: Example comparison of our method and *Wan2.I.*

2106

2107

2108

2109

2110

2111

2112

2113

2114



2115

2116

2117

2118

2119

2120

2121

A young tree sprouts at the front of the house and grows quickly until it stands full-height in front of the facade



2122

2123

2124

2125

2126

2127

2128

2129

2130

A hand reaches into the frame, picks up one cupcake from the row, and removes it until it vanishes from view



2131

2132

2133

2134

2135

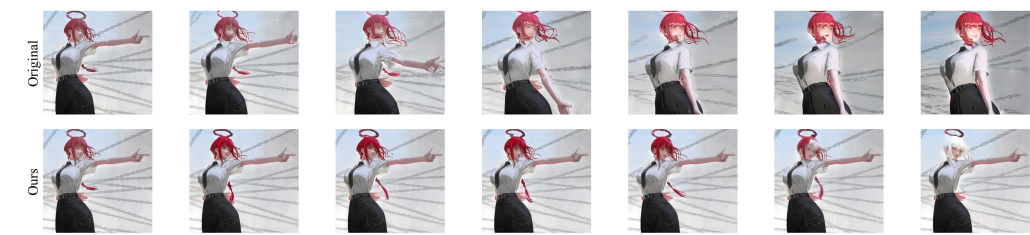
2136

2137

2138

2139

The man extending his arm forward and releasing the diamond from his fingers



2140

2141

2142

2143

2144

2145

2146

2147

2148

2149

2150

2151

2152

2153

2154

2155

2156

2157

2158

2159

Figure 17: Example comparison of our method and *Wan2.1*.

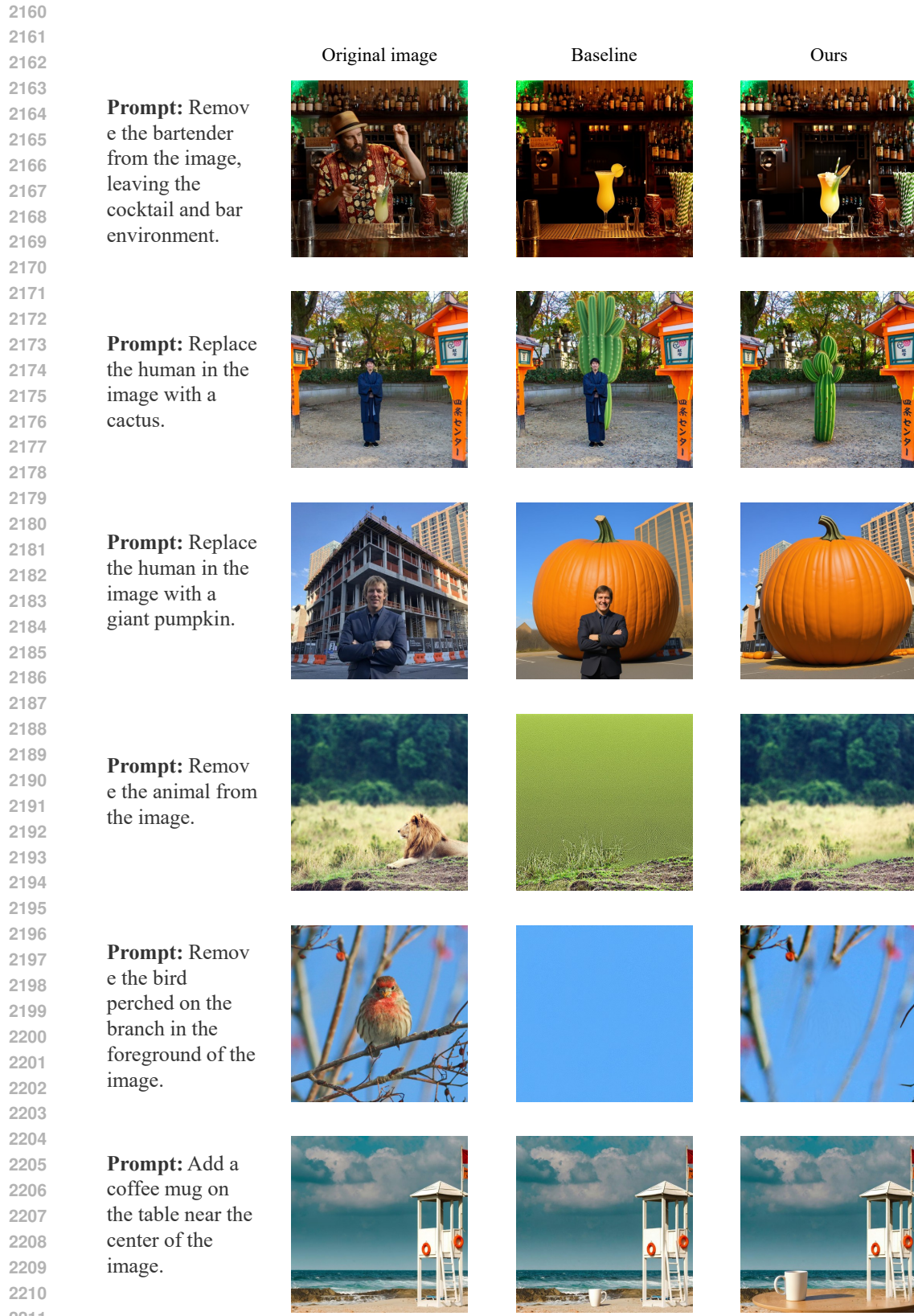
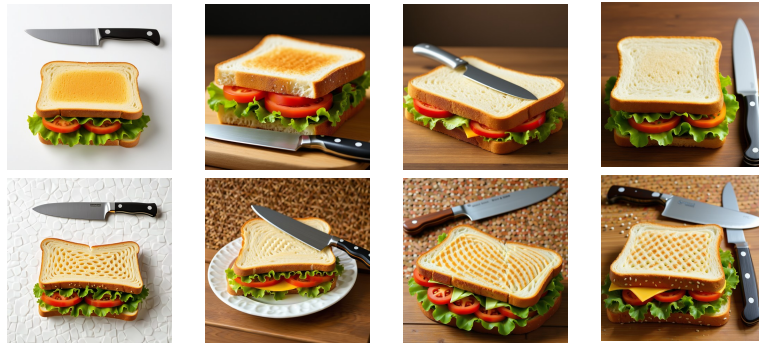


Figure 18: Example comparison of our method and baseline on Imgedit benchmark.

2214
2215
2216
2217
2218
2219
2220
2221
2222
2223
2224
2225

Baseline



2226 **Prompt:** a photo of a sandwich below a knife

2227
2228
2229
2230
2231
2232
2233
2234
2235
2236
2237
2238

Baseline



2239 **Prompt:** a photo of a tie right of a baseball bat

2240
2241
2242
2243
2244
2245
2246
2247
2248
2249
2250
2251

Baseline



2252 **Prompt:** a photo of an elephant below a horse

2253
2254
2255
2256
2257
2258
2259
2260
2261
2262
2263
2264

Baseline



2265 **Prompt:** a photo of a blue clock and a white cup

2266
2267

Figure 19: Example comparison of our method and baseline on Geneval benchmark.

2268

2269

2270 Prompt: a hair drier on the right of a toothbrush front view

2271

2272

2273

2274

2275

2276

2277

2278

2279

2280

2281

2282

2283

2284

2285

2286



Prompt: a handbag and a tie

2287

2288

2289

2290

2291

2292

2293

2294

2295

2296

2297

2298

2299

2300

2301

2302

2303



Prompt: a tie and a suitcase

2304

2305

2306

2307

2308

2309

2310

2311

2312

2313

2314

2315

2316

2317

2318

2319

2320

2321



Figure 20: Example comparison of our method and Wan2.1-T2V-1.3B.

2322

2323

2324

Prompt: an orange on the top of a carrot front view

2325

2326

2327

2328

2329

2330

2331

2332

2333

2334

2335

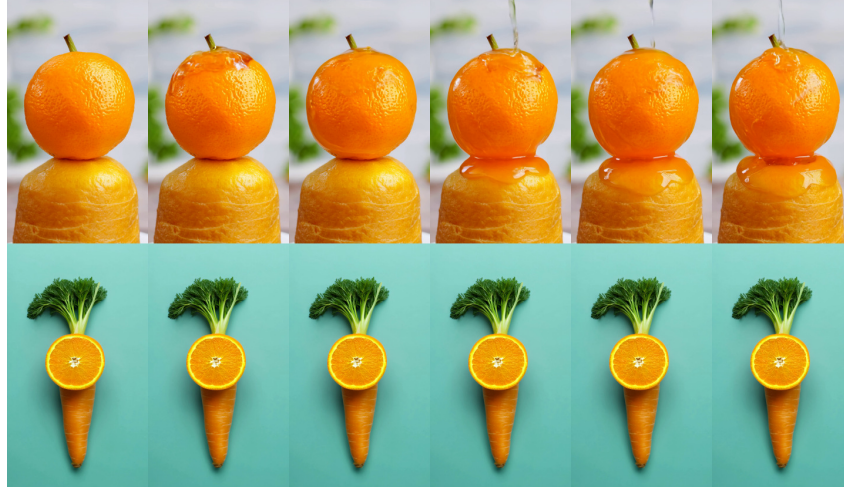
2336

2337

2338

2339

2340



Prompt: an umbrella and a handbag

2341

2342

2343

2344

2345

2346

2347

2348

2349

2350

2351

2352

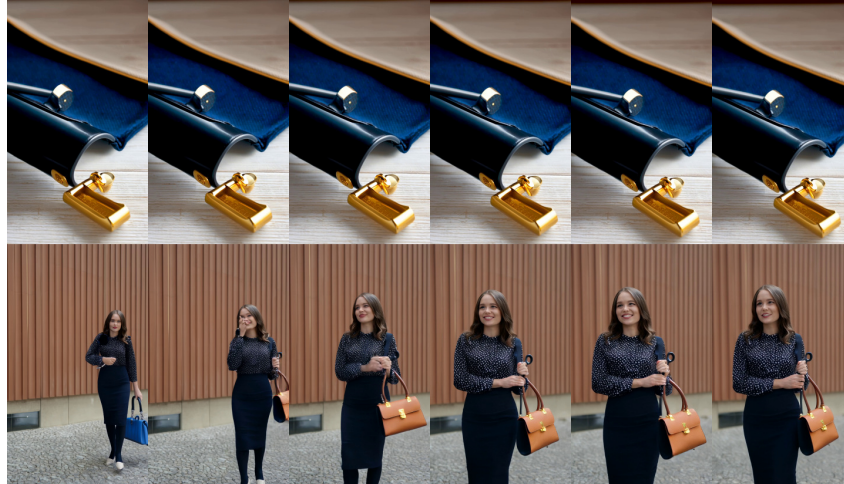
2353

2354

2355

2356

2357



Prompt: skis on the bottom of a snowboard front view

2358

2359

2360

2361

2362

2363

2364

2365

2366

2367

2368

2369

2370

2371

2372

2373

2374

2375



Figure 21: Example comparison of our method and Wan2.1-T2V-1.3B.